Research Square

Preprints are preliminary reports that have not undergone peer review.
They should not be considered conclusive, used to inform clinical practice,
or referenced by the media as validated information.

Resmetirom Reprograms Hepatic Immunometabolism and Fibrotic Remodeling in Mouse Models and Human MASLD

Li Xie
University of Toronto
Xiaofei Nie
University of Toronto
David Dodington
University of Toronto
Heedong Jeon
University of Toronto
Liujun Chen
University of Toronto
Sharvika Bharatselvam
University of Toronto
Lily H. Zhang
University of Toronto
Tao Liang
University of Toronto
Yasaman Ghorbani
University Health Network
Fei Kang
University of Toronto
Toshimasa Takahashi
University of Toronto
Tairan Qin
University of Toronto
Daniel Winer
University Health Network
Shawn Winer
University of Toronto
Juan Domínguez-Bendala
University of Miami Hospital
Mirza Muhammad Fahd Qadir

University of Miami Hospital
Kuanhui Xiang
Peking University
Hoon-Ki Sung
Hospital for Sick Children
Xiaolin He
St. Michael's Hospital
Shukai Huang
St. Michael's Hospital
Kendrix Kek
St. Michael's Hospital
Darren A. Yuen
Hospital for Sick Children
Ori Rotstein
St. Michael's Hospital
Timothy Jackson
University of Toronto
Allan Okrainec
University of Toronto
Johane P. Allard
University of Toronto
Katherine J.P. Schwenger
University Health Network
Herbert Y. Gaisano
herbert.gaisano@utoronto.ca

University of Toronto

Research Article

Keywords: Precision-cut liver slices, metabolic dysfunction–associated steatotic liver disease, Mitochondria, Oxidative phosphorylation, Inflammation, Fibrosis, Extracellular matrix remodeling

Posted Date: November 24th, 2026

DOI: https://doi.org/10.21203/rs.3.rs-11802730/v1

License: This work is licensed under a Creative Commons Attribution 4.0 International License.
Read Full License

Additional Declarations: No competing interests reported.

Resmetirom Reprograms Hepatic Immunometabolism and Fibrotic Remodeling in Mouse Models and Human MASLD

Li Xie[1,2,*], Xiaofei Nie[3], David Dodington[4], Heedong Jeon[1, 2], Liujun Chen[1], Sharvika Bharatselvam[1], Lily H. Zhang[1], Tao Liang[1,2], Yasaman Ghorbani[2], Fei Kang[1, 2], Toshimasa Takahashi[1, 5], Tairan Qin[1], Daniel Winer[4], Shawn Winer[4], Juan Domínguez-Bendala[6], Mirza Muhammad Fahd Qadir[6], Kuanhui Xiang[7], Hoon-Ki Sung[4,8], Xiaolin He[9], Shukai Huang[9], Kendrix Kek[9], Darren A. Yuen[1,9], Ori Rotstein[9,10], Timothy Jackson[10], Allan Okrainec[10], Johane P. Allard[1, 2, 11], Katherine J. P. Schwenger[2], Herbert Y. Gaisano[1, 2, 3,12 *]

[1]Department of Medicine, Temerty Faculty of Medicine, University of Toronto, Toronto, ON, Canada.

[2]Toronto General Hospital Research Institute, University Health Network, Toronto, ON, Canada.

[3]Department of Physiology, Temerty Faculty of Medicine, University of Toronto, Toronto, ON, Canada.

[4]Department of Laboratory Medicine & Pathobiology, University of Toronto, Toronto, ON, Canada

[5]Department of Geriatric and General Medicine, Osaka University Graduate School of Medicine, Osaka, Japan

[6]Diabetes Research Institute, Departments of Cell Biology and Anatomy and Surgery, University of Miami Miller School of Medicine, Miami, FL, USA.

[7]Department of Microbiology and Infectious Disease Center, School of Basic Medical Sciences, Peking University Health Science Center, Beijing 100191, China

[8]The Hospital for Sick Children Research Institute, Toronto, ON, Canada

[9]Keenan Research Centre for Biomedical Science, Li Ka Shing Knowledge Institute, St. Michael's Hospital (Unity Health Toronto), Toronto, ON, Canada

[10]Department of Surgery, University of Toronto, Toronto, ON, Canada

[11]Department of Nutritional Sciences, University of Toronto, Toronto, ON, Canada

[*] Correspondence: li.xie@utoronto.ca; herbert.gaisano@utoronto.ca

Abstract

Background Metabolic dysfunction-associated steatohepatitis (MASH) is characterized by hepatic steatosis accompanied by hepatocellular injury and inflammation. Progression to fibrosis increases the risk of irreversible outcomes of cirrhosis and hepatocellular carcinoma. Resmetirom,

a thyroid hormone receptor β (THRβ) agonist, is the first FDA-approved pharmacological treatment for adults with noncirrhotic MASH and moderate-to-advanced fibrosis (stages F1–F4). However, it's effects on hepatic metabolism, inflammation, and fibrotic remodeling remain unclear and warrant further investigation.

Methods Using precision-cut liver slices (PCLSs) from mice and individuals with obesity undergoing bariatric surgery across different stages of metabolic dysfunction-associated steatotic liver disease (MASLD), we investigate the therapeutic effects and underlying mechanisms.

Results Resmetirom reduced lipid accumulation across a spectrum of hepatic steatosis severity and enhanced mitochondrial function by promoting mitochondrial biogenesis and increasing oxidative phosphorylation capacity. Resmetirom attenuated hepatic stellate cell (HSC) activation and fibrogenesis in human liver slices from patients with fibrosis stages up to F4, as evidenced by coordinated downregulation of fibrotic gene and protein expression. Resmetirom further modulated the MMP2/TIMP1 axis, which led to extracellular matrix (ECM) remodeling and fibrosis regression. Resmetirom also exerted broad anti-inflammatory effects, suppressing the expression and secretion of proinflammatory cytokines and chemokines associated with hepatic immune activation and recruitment.

Conclusion Collectively, these findings demonstrate the multifaceted effects of Resmetirom on hepatic lipid metabolism, mitochondrial function, inflammation, and fibrotic remodeling. We also establish the PCLS from obese patients at different stages of MASLD as a translational ex vivo platform for preclinical drug assessment of specific drug actions and efficacy of potential therapies for MASLD/MASH.

Keywords

Precision-cut liver slices, metabolic dysfunction–associated steatotic liver disease, Mitochondria, Oxidative phosphorylation, Inflammation, Fibrosis, Extracellular matrix remodeling

Introduction

Metabolic dysfunction-associated steatotic liver disease (MASLD) encompasses a spectrum of liver injury characterized by hepatic steatosis that may progress to inflammation (steatohepatitis; MASH), and fibrosis; and is frequently associated with obesity, type 2 diabetes, and other metabolic dysregulation [1-3]. Although several treatments can reduce hepatic fat accumulation [4, 5], only bariatric surgery [6] and, more recently, Resmetirom, a thyroid hormone receptor β (THRβ) agonist [7], followed by the glucagon-like peptide-1 receptor agonist Semaglutide [8] have received United States Food and Drug Administration approval for the treatment of advanced disease (MASH with fibrosis), with evidence of improving fibrosis by at least one stage. Although previous studies have reported the THRβ agonist efficacy on patients with MASH [9,10] a better understanding of the precise cellular mechanisms by which this THRβ agonist targets this multi-stage disease is needed to address the key pathophysiological features of MASLD, including steatosis, mitochondrial function, inflammation, and most importantly, fibrosis which is the primary determinant of mortality [11].

Precision-cut liver slices (PCLSs) provide a superior *ex vivo* model that preserves the liver's three-dimensional architecture and the complex cell-cell interactions that underlie MASLD pathogenesis. PCLSs were prepared from liver samples obtained from obese patients undergoing bariatric surgery; according to our data, approximately 70% of these patients have MASLD at various stages of the condition. Compared to the various rodent models designed to simulate human MASLD,

this model offers direct clinical relevance and translation. Human MASLD PCLSs can genuinely elucidate not only the underlying mechanisms of various MASLD processes but also assess the specific drug actions of candidate drugs and their therapeutic efficacy at each advancing disease stage of MASLD [12] The choice of culture system is a critical strategy to minimize PCLSs hypoxia and to limit the accumulation of toxic metabolites [13]. A perfluorocarbon (PFC)-based system designed to enhance oxygen transfer to three-dimensional tissue preserves pancreatic slice viability and normal function for up to 10 days in culture [14]. We used these PFC dishes to culture human and mouse PCLSs, which similarly extended the health, metabolic and synthetic activities, and functional lifespan of PCLSs to at least 6 days.

We then treated PCLSs derived from both mouse livers and liver tissue from obese patients undergoing bariatric surgery with Resmetirom. To characterize the transcriptional response to treatment, we performed RNA sequencing (RNA-seq), followed by differential gene expression and pathway analyses, comparing Resmetirom-treated and untreated PCLSs. Subsequently, we employed a combination of real-time imaging, biochemical and histological analyses, and western blotting to evaluate the drug's effects on lipid accumulation, mitochondrial function, inflammatory responses, hepatic stellate cell (HSC) activation, as well as the resulting fibrotic response and its resolution. Furthermore, this study demonstrates that obese patient-derived PCLS can serve as a translational preclinical platform for assessing drug efficacy prior to clinical trials.

Material and methods

Ethics Approval

All animal procedures complied with the University of Toronto's Animal Care Committee guidelines and were approved under institutional animal use protocols (University Health Network (UHN), Toronto, ON, Canada) in accordance with the Canadian Council on Animal Care Standards and the Animals for Research Act of Ontario. Human tissue studies were approved by the UHN Research Ethics Board (REB#24-5175), the Unity Health Ethics Board (REB#23-234) and the Research Ethics Committee of the University of Toronto (permit no. 40437). All research was conducted in accordance with both the Declarations of Helsinki and Istanbul and all participants provided written and informed consent.

Animals

Housing and Husbandry: Animals were cared for and housed in the animal facility at the Division of Comparative Medicine (DCM), University of Toronto, with approved Animal Use Protocol 20012986. C57BL/6 mice were maintained on a 12 h light/dark cycle at constant ambient temperature (22–23 °C) and fed standard chow and water ad libitum with nesting materials.

Strain and Transgene: Col1A1-GFP mice were originally obtained from Dr. Hidekazu Tsukamoto's lab (Keck School of Medicine of the University of Southern California, Los Angeles, CA).

Human Liver Tissue

This study includes subjects living with obesity (BMI ≥35 kg/m^2) who underwent bariatric surgery at the Toronto Western Hospital and Unity Health/Saint Joseph Hospital; both in Toronto, Canada. Individuals were approached by a research coordinator on the day of bariatric surgery, and a liver biopsy was taken during surgery. A portion prepared for histology and the remaining larger portion

for PCLS preparation. A breakdown of the patients clinical and histological data can be found in Table 1.

Precision-Cut Liver Slices (PCLSs) preparation and culture

Mouse or human liver tissue was cut into approximately 5 mm pieces and transferred to 35 mm dishes, submerged in 3% low melting point agarose (ThermoFisher; #16520100), and placed on ice for 20 minutes. Agarose embedded liver cores were superglued to the vibratome mounting stage, submersed in the chamber containing 4°C extracellular solution [15], and cut using a Leica VT1200S vibrating blade microtome (Leica Biosystems Canada) at a speed 0.2 mm/sec, amplitude 1 mm, and thickness of 100-200 µm. PCLSs were transferred into regular cell culture dish or air-permeable perfluorocarbon (PFC) membrane culture dishes (Biorep Technologies, Miami Lakes, FL). All PCLSs were cultured in Williams' medium E (Sigma-Aldrich; #W4128), supplemented with 1% penicillin/streptomycin and l-glutamine, 1×insulin transferrin-selenium X (ThermoFisher; #41400045), and 2% fetal bovine serum (Corning; #35-076-CV) at 37°C, supplemented with 5% CO_2.

Real-time imaging on PCLSs

A cultured piece of live PCLS (100-200 µm thickness) was brushed into an imaging chamber (bottom coverslip #1) containing PBS solution and a tissue slice anchor (Harvard Apparatus, Holliston, MA) applied to stabilize the slice. The imaging was conducted on a Quorum spinning disk confocal microscope (Olympus IX81; Tokyo, Japan) in the imaging facility at the Hospital for Sick Children (Toronto, Canada). The images are analyzed using ImageJ software.

Histopathology

Human Liver Tissue: A small piece of liver tissue was cut from the patient's liver sample, fixed with 10% formalin, embedded in paraffin, cut into 4-µm-thick sections, and stained with standard hematoxylin and eosin (H&E) and Masson's trichrome (The Center for Phenogenomics, Toronto). Images were taken with a Hamamatsu NanoZoomer S360 at 20x magnification. Based on the staining images, the liver pathologists evaluated the samples using the Brunt system [16], and summarized the data for macrovesicular steatosis, MASLD activity score (NAS), steatosis grade, lobular inflammation, ballooning, portal inflammation, and fibrosis stage (Table 1). MASLD was diagnosed if the liver had >5% steatosis, and MASH was confirmed when ballooning of hepatocytes was present. Fibrosis stage was designated according to the Brunt scoring system (F0 to F4), where stage 0 = no fibrosis, stage 1 = mild fibrosis, stage 2 = moderate fibrosis, stage 3 = severe fibrosis, and stage 4 = cirrhosis. The histology preparation and pathology reading were performed after slice assays, and therefore the latter were performed 'blinded' with regards to the liver histology.

PCLSs (fibrogenesis assays): Cultured PCLSs (200 -250 µm thick) were treated with the profibrotic stimuli TGFβ1 and PDGF-BB (ThermoFisher; Cat# 100-21; # 315-18), with or without Resmetirom (MedChemExpress; # HY-12216), for 3 days. Following treatment, PCLSs were fixed in 4% paraformaldehyde, processed, and subjected to histological and immunohistochemical analyses. Hematoxylin and eosin (H&E) staining was performed to assess overall tissue morphology, while Picrosirius red (PSR) staining was used to evaluate collagen fiber distribution and deposition. Immunohistochemical staining for α-smooth muscle actin (α-SMA), using an anti-α-SMA antibody (clone 1A4; ThermoFisher; #14-9760-82), was performed to assess myofibroblast activation. The Center for Phenogenomics in Toronto employed a special strategy for histology preparation, using the agar sandwich plus tissue dye method to process and embed

cultured human PCLSs. Images were taken with a Zeiss Slide Scanner Axioscan 7 at 20x magnification. Digital slides were analyzed using HALO software (Melbourne, FL, USA) at the SickKids Hospital Research Institute (Toronto, Canada).

Biochemical Assays

Albumin assay: To measure PCLSs' viability, mouse albumin assay kit (Abcam; #ab207620) or human albumin assay kit (ThermoFisher; #EHALB) were used following manufacturer's instruction. Supernatants were collected at 24 or 48 h intervals, and PCLSs were harvested for histological assay.

Hepatic Triglycerides: To measure hepatic triglyceride (TG) content, Triglyceride Colorimetric Assay Kit (Cayman; cat#10010303) was used following manufacturer's instruction. Briefly, 100 mg of mouse liver slices were harvested from each condition after 2 days of culture. And then washed with cold PBS and homogenized in diluted NP40 Substitute Assay Reagent containing protease inhibitor. Tissue homogenates were then centrifuged at 10,000 × g for 10 min at 4 °C. Samples were diluted and then incubated with Enzyme Mixture solution for 60 min at room temperature to initiate the reaction and the absorbance was measured at 540 nm using a microplate reader (Bio-Rad, ON, Canada).

ATP quantification: ATP content in PCLSs was quantified with ATP determination kit (ThermoFisher, #A22066). This ATP assay kit utilizes the reaction between recombinant firefly luciferase and its substrate D-luciferin and is based on luciferase's absolute requirement for ATP in producing light (emission maximum approximately 560 nm at pH 7.8). Briefly, 8–10 liver slices from each condition were collected after 1 day of culture with or without Resmetirom (50 μM), washed with cold PBS, and homogenized in ATP assay buffer provided in the kit (30 mg tissue per

100 µL buffer), followed by centrifugation at 12,000 g in cold for 5 min. Supernatant was transferred to new tubes and ATP was quantified using PHERAstar FS microplate reader (BMG Labtech; Mandel Scientific Company Inc., Guelph, ON, Canada). ATP concentrations (nM) from experimental samples were calculated and normalized to the corresponding protein concentrations (mg/mL).

Hydroxyproline (collagen) Quantification: Hydroxyproline content was measured using a commercial assay kit (Abcam; #AB222941), following the manufacturer's protocol. Briefly, tissue was homogenized (10 mg per 100 µL ddH_2O) and hydrolyzed with the addition of 100 µL of 10 N concentrated NaOH to 100 µL of the sample followed by heating at 120°C for 3 hours. After alkaline hydrolysis, the vials were placed on ice to cool. Then, 100 µL of 10 N concentrated HCl was added to neutralize residual NaOH. The samples were then vortexed followed by centrifugation at 10,000g for 5 minutes to pellet insoluble debris. Supernatant was then heated at 65°C to enable evaporation, and then chloramine-T concentrate was added to the wells and incubated at room temperature for 20 minutes. To visualize hydroxyproline concentration, 50 µL of developer solution was added to each well and incubated at 37°C for 5 minutes, followed by addition of 50 µL of DMAB concentrate solution and incubation at 65°C for 45 minutes. Sample absorbance was measured at 560 nm using a microplate reader (Bio-Rad). A standard curve was generated using known concentrations of trans-4-hydroxyl-L-proline. Hydroxyproline concentrations from experimental samples were then calculated and normalized to 1 mg of wet liver tissue.

Human Pro-Collagen Iα1 assay: Human Pro-Collagen Iα1 DuoSet ELISA kit (R&D Systems; #DY6220-05) was used to detect and quantify pro-collagen 1A1 in the medium as a marker of

newly produced collagen 1α1. Human PCLSs or human primary HSC culture medium were collected and followed the manufacturer's protocol.

Meso Scale Discovery (MSD) multiplex assay

Protein levels were measured using MSD multiplex electrochemiluminescence assays according to the manufacturer's instructions (Meso Scale Disvcovery, Rockville, Maryland, US). Samples and standards were added to pre-coated multi-spot plates and incubated with analyte-specific capture antibodies. After washing, SULFO-TAG–labeled detection antibodies were applied. Electrochemiluminescent signals were detected using an MSD instrument (MESO QuickPlex SQ 120MM) and quantified against analyte-specific standard curves.

Single cell isolation from mouse liver

Mice were anesthetized, and the chest cavity was opened to catheterize the superior vena cava (SVC) through the right atrium. The catheter was secured and connected to the afferent tubing for perfusion. Livers were perfused sequentially with HBSS containing EDTA, followed by 0.626 mg/mL collagenase P in DMEM/F-12, and then 10 µg/mL DNase I in DMEM/F-12. Different liver cell populations were subsequently separated by gradient ultracentrifugation.

Cell line

Generation of *LX2-Col1A1-GFP Reporter Cell Line:* To establish a reporter cell line for collagen expression, LX2 hepatic stellate cells were transduced with a lentiviral vector encoding GFP under the control of the human Col1A1 promoter and containing a puromycin resistance cassette. The Col1A1-GFP construct was generously provided by Dr. Kuanhui Xiang (Peking University, China) [17]. Lentiviral particles were produced in HEK293T cells using a standard three-plasmid packaging system. Viral supernatants were collected at 72 hours post-transfection and used to

infect LX2 cells at ~40% confluence. Puromycin selection (1.5 μg/mL) was initiated 48 hours post-infection and maintained for 7–10 days until non-transduced cells were eliminated. Surviving cells were expanded under maintenance puromycin (1 μg/mL), and GFP expression was verified by fluorescence microscopy.

Human primary hepatic stellate cells

Human hepatic stellate cells (hHSCs; #CSC-C1496) were purchased from Creative Bioarray (New York, USA) and cultured in Hepatic Stellate Growth Medium (Creative Bioarray; #CM-C1496) in a humidified incubator maintained at 37°C with 5% CO_2. Cells were seeded in 6-well plates at a density of 0.2×10^6 cells/well. On day 2, cells were serum-starved for 1 h and pretreated with vehicle or Resmetirom (30 μM) for an additional 1 h. The culture medium was then replaced with DMEM/F12 containing either vehicle (0.1% DMSO), TGFβ1 (5 ng/mL) alone, TGFβ1 (5 ng/mL) in combination with Resmetirom with different dosed. After 48 h of treatment, culture supernatants were collected for measurement of secreted procollagen type I α1 (procollagen Iα1) using a human Procollagen Iα1 DuoSet ELISA kit.

Quantitative PCR (qPCR)

Total RNA was extracted from mouse liver slices using the PureLink RNA mini kit (Thermo Fisher) following the manufacturer's manual. cDNA was synthesized using iScriptTM cDNA synthesis kit (Bio-Rad, Cat#1708891) and qPCR reaction was run with PowerUP SYBR Green Master Mix (Applied Biosystem, Cat#A25741) in Bio-Rad CFX Connect Real Time PCR Detection system. Relative expression levels of each gene were calculated using the 2-ΔCt method. The primers used were as follows:

Mouse Acta2 forward: 5'-CACTGAACCCTAAGGCCAAC-3'

Mouse Col1a1 forward: 5'-GAACAAGGTGACAGAGGCATA-3'

Mouse Timp1 forward: 5'-TCTTGGTTCCCTGGCGTACTCT-3'

Mouse GAPDH forward: 5'-ATGTGTCCGTCGTGGATCTGA-3'

Western blotting

PCLSs or primary human HSCs were homogenized in RIPA buffer containing protease and phosphatase inhibitors. Protein concentrations were determined using the BCA assay. Equal amounts of protein (15-20 μg) were resolved by SDS-PAGE and transferred to PVDF membranes. Membranes were probed with antibodies against ETC components, α-SMA, MMP2, TIMP1 and GAPDH (loading control). Bands were visualized using ECL substrate and imaged on a ChemiDoc MP system (Bio-Rad).

RNA Sequencing (RNA-seq)

Total RNA was isolated from mouse and patient liver slices using the Zymo RNA Miniprep Kit (Zymo Research, VWR) and PureLink RNA mini kit (Thermo Fisher, Canada) following the manufacturer's protocols. RNA integrity number (RIN), rRNA ratio, and sample concentration were assessed using an Agilent 2100 Bioanalyzer (Agilent Technologies). RNA from mouse PCLSs using mRNA library preparation (poly A enrichment) and total RNA was subsequently sequenced on NovaSeq X Plus Series (PE150; 20M paired reads/6 G raw data per sample; Novogene, CA, USA). RNA from patient PCLSs using the Kapa Hyperprep RNA library prep with Riboerase and total RNA was subsequently sequenced on Illumina Novaseq X-Plus 25B flow cell (PE150; 40M paired reads/12Gb raw data per sample; Novogene, CA, USA). RNA-seq data were analyzed using R software. Differential gene expression analysis between two groups was

performed using the DESeq2 package on raw count data, applying internal size-factor normalization and negative binomial generalized linear modeling[7]. Differentially expressed genes (DEGs) were defined by an adjusted *P* value < 0.05 using the Benjamini–Hochberg method. Functional annotation and enrichment analyses were conducted using the clusterProfiler package[8]. Statistical inference was based on model-derived log2 fold changes, while normalized expression values were used exclusively for visualization relative to control samples.

Quantification and statistical analysis

The number of mice and patients used in experiments are described within the associated figure legend. All statistical calculations were performed using GraphPad Prism 8 software (GraphPad Software, USA). Data were analyzed using one-way ANOVA with Dunnett's multiple comparison or unpaired two-tailed Student's t-tests as indicated in figures. *p* values less than 0.05 were considered significant (*$p \leq 0.05$, **$p \leq 0.01$, ***$p \leq 0.001$). Error bars represent mean ± s.e.m. *p* values, exact sample sizes and statistical tests are provided in the associated figure legends for each figure.

Results

Resmetirom reverses hepatic steatosis and improves mitochondrial function and biogenesis in mouse livers

Excess hepatic *de novo* lipogenesis (DNL) is a hallmark of MASLD, and contributes to lipotoxicity, inflammation, and fibrosis [18]. To assess the effect of Resmetirom on steatosis, liver tissue from normal mice were cut into 120 μm thickness slices, these PCLSs were then cultured in air-permeable perfluorocarbon (PFC) culture dishes to ensure viability over a period of 6 days, which

is required for our live-cell imaging and fibrosis assays (Fig. 1A). Mouse PCLS albumin production remained stable over the 6-day culture period in PFC dishes which compared to Day 2 showed a reduction of 15% at day 3, 28% at day 4 and 40% at day 6, whereas albumin levels in PCLS cultured on regular dishes decreased by 68% after 3 days and decreased further compared with time-matched PFC-cultured PCLSs (Fig. 1B). DNL was induced in normal mouse PCLSs (Fig. 1C) using high glucose (25 mM) and insulin (1.7 µM) for 48 hours [19] and slices were additionally treated with or without Resmetirom (50 uM). Lipid droplets were visualized by real-time imaging after 30 minutes of incubation with green BODIPY.

On normal mouse PCLSs, compared with control condition (11 mM glucose, no insulin), high glucose and insulin increased lipid accumulation in mice to 3.6-fold (% area) and lipid droplet size to 2.2-fold (pixel^2). In contrast, Resmetirom reduced DNL, as evidenced by a 40% decrease in lipid accumulation and a 29% decrease in lipid droplet size (Fig. 1D). Similarly, triglyceride assay confirmed that Resmetirom reduced triglycerides content to near baseline level (Fig. 1E). Meanwhile, based on RNA-seq data from mouse PCLS, we found that Resmetirom does not affect the expression of genes involved in lipid synthesis, but it upregulates the expression of genes related to fatty acid oxidation (FAO), including carnitine palmitoyltransferase 1A (*Cpt1a*) and fibroblast growth factor 21 (*Fgf21*) (Fig. 1H). These results indicate that Resmetirom promotes a shift in hepatic lipid metabolism from *de novo* lipogenesis toward fatty acid oxidation.

Mitochondria are crucial for liver function, supporting energy production, FAO, urea synthesis, and detoxification [20]. To assess whether Resmetirom promotes mitochondrial biogenesis, we used acetaminophen to induce mitochondrial damage [21] and then used the terminal enzyme of the electron transport chain (ETC), cytochrome c oxidase subunit 8 (COX8), to track mitochondrial abundance, turnover, and mitophagy [22] by tagging mCherry and GFP to the N- and C-terminals

of COX8. PCLSs from mice infected with Ad-COX8-mCherry/GFP were treated with acetaminophen (5 mM) for 24 hr to induce severe mitochondrial damage. Starting at 3 hr and reaching a maximum at 12 hr, damaged mitochondria that underwent mitophagy and were delivered into autolysosomes displaying red fluorescence (mCherry), as the acidic lysosomal pH quenched the green fluorescence (EGFP). Surprisingly, a 12-hr treatment of 50 μM Resmetirom added after 12-hr of acetaminophen treatment promoted the formation of new mitochondria, which appeared as increased green fluorescence at 24 hr (Fig. 1F). Acetaminophen treatment reduced this ratio to 40% of baseline, whereas resmetirom restored GFP fluorescence, increasing the GFP/mCherry ratio to 1.05, comparable to control levels (Fig. 1G). This recovery is interpreted as evidence of new mitochondrial biogenesis, since approximately 60% of the pre-existing mitochondria were destroyed after 24 hr of acetaminophen treatment. The protection against acetaminophen injury is particularly significant because acetaminophen toxicity is known to cause severe mitochondrial damage, especially in MASLD patients [21]. Consistent with the imaging results, Resmetirom significantly increased expression of genes involved in energy sensing and mitochondrial biogenesis, such as protein kinase AMP-activated non-catalytic subunit beta 1 (*Prkab1*) and peroxisome proliferator-activated receptor gamma coactivator-1 beta (PGC-1β, *Ppargc1b*) in mouse PCLSs (Fig. 1H). Oxidative phosphorylation (OXPHOS) in liver mitochondria relies on nuclear- and mitochondrial-encoded genes that regulate the electron transport chain (ETC) and ATP synthesis. We used Seurat's module score function to model global OXPHOS related genes [23]. The module showed that Resmetirom upregulated the global OXPHOS genes (Fig. 1I).

RNA-seq data analysis shows the differential gene expression and enrichment pathways from mouse PCLSs. PCA ratio between control and Resmetirom-treated groups (Fig. 1J). A volcano

plot was used to visualize differential gene expressions between the control and Resmetirom treatment groups (Fig. 1K). Genes with |log2FC| > 1 and adjusted p-value < 0.05 are highlighted in red (upregulated) and blue (downregulated), representing the most significantly altered genes. Several key metabolic and inflammatory genes were strongly modulated, appearing at the extremes of the plot, suggesting robust transcriptional changes induced by the treatment. Dot plot of enriched GO biological processes for differentially expressed genes (DEGs), in which immune response, lipid transport, and oxidative phosphorylation were among the top enriched processes. Dot plot of enriched KEGG pathways related to oxidative phosphorylation, immune signaling, viral infection, and metabolic processes were prominently enriched (Fig. 1L).

Resmetirom reverses hepatic steatosis and improve mitochondrial function in obese patient livers

Livers from obese patients, which unlike mice, are heterogeneous and at different stages of MASLD, particularly in the severity of fat accumulation (Fig. 2). First, we show patient liver slices cultured in PFC dishes at different times and performed H&E staining to show maintenance of tissue health and albumin determination to show intact secretory function (Fig. 2A, B) comparable to the mouse PCLS results, which was a mild reduction of 17% at day 3 and 38% at day 5 compared to day 1. We present three representative patient cases at increasing severity of steatosis. Donor 1 (female, age 28, BMI 54) has a liver with very mild steatosis (<5%, Fig. 2C, top). Compared with control condition (11 mM glucose, no insulin), DNL stimulation increased lipid accumulation in donor 1 to 3.4-fold (% area) and lipid droplet size to 1.3-fold (pixel^2). In contrast, Resmetirom attenuated the stimulated DNL levels to baseline (Fig. 2D, top). Donor 2 (female, age 49, BMI 39) has mild steatosis (20%, Fig. 2C, middle) with mild MASH (NAS 2/8). DNL stimulation increased lipid accumulation in donor 2 to 1.7-fold and lipid droplet size to 1.7-fold, whereas Resmetirom

reduced stimulated DNL lipid accumulation and droplet size to baseline levels (Fig. 2D, middle). Donor 3 (female, age 51, BMI 42) has a more severe steatosis (40%, Fig. 2C, bottom**)** with more severe MASH (NAS 4/8) and stage 1 fibrosis. DNL stimulation increased lipid accumulation to 1.8-fold and lipid droplet size to 1.9-fold, whereas Resmetirom again returned stimulated DNL levels to baseline (Fig. 2D, bottom). These findings demonstrate that Resmetirom can reduce lipogenesis by decreasing both lipid accumulation and lipid droplet size in hepatocytes of mild to severe cases of steatosis.

Furthermore, ATP assay of PCLS from MASLD/MASH patients showed that Resmetirom enhanced mitochondrial function by increasing ATP levels (Fig. 2E). Western blot results further show that Resmetirom enhances the protein expression from ETC complex units especially unit V and III (Fig. 2F). These changes suggest that THRβ activation by Resmetirom primes hepatocyte energy sensing and drives coordinated mitochondrial biogenesis (taken together with the mouse data in Fig. 1F-G) and oxidative metabolism.

Resmetirom reverses *de novo* fibrogenesis and reduces inflammation in mouse PCLSs

PCLSs were generated from healthy mouse livers. After 24 hr of culture, these PCLSs were stimulated for up to 72 hr in the presence or absence of profibrotic stimuli TGFβ1/PDGF-BB (5 ng/mL + 5 ng/mL) and with or without Resmetirom (50 μM). H&E staining demonstrated that PCLSs maintained a healthy morphology over a 4-day culture period (Fig. 3A, left). PSR staining revealed collagen deposition within the fibrotic matrix of PCLSs (Fig. 3A, right). In healthy mouse PCLSs at t = 0, PSR staining was confined to vascular structures. After 4 days of culture under control conditions, PSR staining revealed collagen thickening around central veins and mild perisinusoidal deposition; however, quantitative PSR area analysis demonstrated only a minor, statistically insignificant increase in collagen content compared with time-matched t = 0 mouse

PCLSs. Conversely, TGFβ1/PDGF induced more extensive perisinusoidal fibrosis, with thick multilayered collagen present around vessels and increased collagen deposition in all mice (2.4-fold) compared to the control cultured PCLSs (96 hr), but this was significantly attenuated and comparable to control levels after Resmetirom treatment (Fig. 3A, B). Similarly, Hydroxyproline assay was used to quantify collagen content in tissues and further demonstrated that profibrotic stimuli increase hydroxyproline content (2.3-fold compared to 96 hr control), indicating increased collagen biosynthesis and deposition of extracellular matrix, but Resmetirom significantly reduced it to control levels (Fig. 3C). At the transcriptional level, we found the expression levels of the profibrotic gene *Col1A1*, HSC activation marker *Acta2*, and tissue inhibitor of metalloproteinase 1 (*Timp1*) were significantly upregulated after 72 hr of TGFβ1/PDGF stimulation. However, this overexpression was markedly suppressed by Resmetirom treatment (Fig. 3D). In parallel, RNA-seq analysis demonstrated that key fibrotic genes, including *Col1a1, Acta2, Timp1, Tgfb2, Tgfb1i1* and *Ccn2,* were consistently downregulated by Resmetirom in mouse PCLSs (Fig. 3E). Seurat's module score function showed that Resmetirom downregulated global fibrotic-related genes (Fig. 3F). GSEA was performed on the sorted gene expression dataset from mouse RNA-seq data. The enrichment score (ES, black curve) reaches a negative peak, indicating that these gene sets are enriched among downregulated genes and regulate tissue remodeling (Fig. 3G).

Chronic liver disease leads to hepatocellular injury that triggers a pro-inflammatory state resulting in liver fibrosis, cirrhosis, portal hypertension and liver failure. Liver inflammation is understood as a complex process driven by several key gene groups that coordinate the transition from MASLD to MASH and fibrosis. RNA-seq analysis revealed that Resmetirom treatment significantly downregulated multiple inflammatory gene programs, including pro-inflammatory cytokines (*Il1b* and *Il6*), chemokines and their receptors (*Ccl2, Ccl5, Ccl8, Ccl12, Ccr5, Cxcl9,*

Cxcl10 and *Cxcl16*), as well as innate immune and inflammasome-related genes (*Tlr4, Nlrp3* and *Irf7*) in mouse PCLSs (Fig. 3E). The module score showed that Resmetirom downregulated the global inflammatory-related genes (Fig. 3F). GSEA shows that ES (green curve) reaches a negative peak, indicating that these gene sets are enriched among downregulated genes and regulate cytokine-mediated signalling pathway (Fig. 3G). Taken together, these results demonstrate that Resmetirom broadly suppresses hepatic inflammatory signaling pathways associated with MASH progression and fibrosis development, and reverses fibrosis by capturing its direct suppressive effects on core fibrogenic gene programs.

Resmetirom reverses fibrosis progression across different stages in MASLD patient livers

Whereas Resmetirom was reported to reduce fibrosis by one stage in MASH/MASLD patients, it was only by a net 12% (25.9% vs placebo control of 14.2%) of the MASLD patient population [7]. It is therefore very important to devise a strategy that could assess responders vs non-responders at the different stages of fibrosis. We directly conducted histology analysis on liver slices from a large number of obese patients undergong bariatric surgery and classified them into the different stages of fibrosis (3-7 patients for each stage of F0, F1, F2 and F3/F4), degree of steastosis and NAS scores. Compared with t=0 control condition, PSR-positive area is higher after culture which may indicates that culture induces a mild wound-healing or fibrogenic response; consenquently, PCLS cultured for 4 days can contain more newly deposited or remodeled collagen than the freshly prepared liver slices (Fig. 4A, B). However, fibrotic changes with TGFβ1/PDGF treatment further induces more intense and extensive perisinusoidal PSR staining, accompanied by thickened collagen deposition throughout the tissue surface and around the vessels. In contrast, profibrotic stimuli induced hepatic myofibroblast activation and collagen deposition was attenuated by Resmetirom, and the histological appearance was similar with 96 hr control PCLSs (Fig. 4A shows

the representative examples for F0 to F3; the precise description of the histology of each patient donor is shown in Table 1). Quantitative PSR area analysis revealed that profibrotic stimuli significantly increased collagen deposition in all donors (Fig. 4B shows the results of 3-7 patient donors for each of F0 to F3/F4). Co-treatment with Resmetirom (50 μM) attenuated this effect in all patient livers, resulting in collagen levels comparable to those of the control livers (summaries in Fig. 4B). Moreover, we found that Resmetirom was able to reduce new fibrosis development induced by profibrotic stimuli not only in no fibrosis (F0, with NAS 1/8) and mild fibrosis patient livers (F1, with NAS 0/8; and F2, with NAS 4/8), but remarkably also in severe fibrosis patients (F3/F4, with NAS 4/8; Fig. 4B). Further analysis of Fig. 4B revealed the average PSR-positive area across different stages of fibrosis, illustrating the overall trajectories of collagen deposition (Fig. 4C). These *ex vivo* results are consistent with reported clinical trial results of Resmetirom [7]. In parallel, Resmetirom reduced pro-collagen 1A1 production in patient liver slices stimulated with TGFβ1/PDGF, indicating that Resmetirom inhibited new collagen synthesis (Fig. 4D). Similar results were obtained when examing αSMA stained sections (Fig. 4E, F). These findings suggest that Resmetirom can reduce new fibrosis development and reverse it to a milder stage in liver slices of bariatric surgery patients even in those with advanced MASH and fibrotic stage, thus supporting Resmetirom treatment for more severe stages of hepatic fibrosis.

Resmetirom can bypass hepatocyte-mediated effects and act directly on hepatic stellate cells

Hepatic fibrosis in MASH is believed to be largely caused by prolonged inflammation and activation of hepatic stellate cells (HSC) and collagen-secreting myofibroblasts [24]. In response to liver injury and inflammation, resident macrophage Kupffer cells secrete TGFβ1, which, together with PDGF released predominantly by platelets, serves as a principal driver of HSC activation and hepatic myofibroblast proliferation and survival [25, 26]. We assessed HSC

activation using Col1A1-GFP transgenic mice carrying the fluorescent Col1A1 promoter [27]. PCLSs were prepared from Col1A1-GFP transgenic mice and subjected to stimulation for 48 h. The live imaging of PCLSs revealed that fibrosis induction with TGFβ1/PDGF increased the number of HSCs (more GFP cells) and most of these activated HSCs showed morphological changes from the quiescent state (small round or stellate shape) to activated conformation (larger, flatter, cytoplasmic extensions). In contrast, co-treatment with Resmetirom reduced the number of fluorescent HSCs with their fluorescence intensity and morphological changes similar to quiescent HSCs with decreased cell size appearing spindle shaped or round (Fig. 5A-D). Meanwhile, high-magnification imaging demonstrated robust upregulation of α-SMA protein in HSCs under profibrotic stimulation, whereas α-SMA was not detected in control or Resmetirom-treated mice PCLSs (Fig. 5C).

Furthermore, to determine whether Resmetirom can bypass hepatocyte-mediated effects and act directly on HSCs, we isolated primary HSCs from Col1A1-GFP mice. Previous studies have reported that HSCs express both THRα and THRβ, with THRα exhibiting higher expression than THRβ, suggesting that Resmetirom may exert direct effects on HSCs through THRα [28]. Profibrotic stimuli plus Resmetirom treatment did not induce α-SMA expression compared to profibrotic stimuli alone, indicating that Resmetirom can directly inhibit HSC activation (Fig. 5D, E; Fig. S1A). In addition, Col1A1-GFP was also stably expressed in a human HSC line (LX2) [17]. Here, Resmetirom similarly inhibited HSC activation by reducing GFP intensity and blunting HSC morphological changes in the Col1A1-GFP LX2 stable cell line (Fig. S1B, C).

Moreover, we utilized commercially available primary human HSCs and transduced them with lenti-Col1A1-GFP lentivirus. The results showed that Resmetirom treatment reduced α-SMA fluorescence intensity, Col1A1 expression level, decreased cell volume, and increased cell

circularity compared to profibrotic stimulation alone (Fig. 6A, B). In addition, western blot results showed that treatment with Resmetirom alone downregulated α-SMA expression in human HSCs compared with the vehicle control group (Fig. 6C). Concurrently, Resmetirom dose-dependently reduced the production of procollagen 1A1 in TGFβ1-stimulated human HSCs (Fig. 6D), with effective dose range of 30 – 100 μM Resmetirom, which confirms the effective dose of 50 μM Resmetirom we have used in PCLSs. Taken together, these results indicate that Resmetirom can directly prevent the activation of human HSCs, thereby inhibiting the progression of liver fibrosis.

Resmetirom reduces inflammatin and promotes ECM remodeling and fibrosis degradation

Consistent with the mouse RNA-seq data, we found that treatment of PCLS from MASLD patient donors with Resmetirom also downregulated the expression of fibrosis-related genes (*Col1A1, TGFB1, TGFb1I1, PDGFR* and *CCN2*) (Fig. 7A), and multiple inflammatory gene programs, including pro-inflammatory cytokines and chemokines (*IL1b, IL6 CCL2, CXCL1, CXCL2, CXCL10* and *CXCL11*) in patient derived PCLSs (Fig. 7B). To confirm the regulation of inflammatory mediators at the protein level, multiplex cytokine and chemokine profiling was performed on culture media from patient PCLSs treated with or without Resmetirom using the MSD U-PLEX platform. A custom U-PLEX panel targeting seven mediators, IL-1β, IL-6, MCP-1 (*CCL2*), GRO-α (*CXCL1*), MIG (*CXCL9*), IP-10 (*CXCL10*), and I-TAC (*CXCL11*), was employed. Resmetirom vigorously suppressed the secretion of all detected mediators (Fig. 7C), including MIG (*CXCL9*), which did not exhibit significant differential expression at the transcriptomic level, suggesting post-transcriptional or secretion-level regulation.

Next, we evaluated whether Resmetirom can alleviate established fibrosis and promote ECM remodeling. We first employed a high fat diet (HFD) mouse model, in which 8-week-old C57BL/6 mice were fed a choline-deficient, L-amino acid-defined, 60% fat diet (Research Diets A06971302;

New Brunswick, NJ) for 16 weeks. This model reliably induces MASH accompanied by mild fibrosis [29]. In these fibrotic mouse livers, we observed that treatment of PCLSs with Resmetirom alone resulted in a 30% reduction in the PSR-positive area (Fig. S2). Subsequently, in liver slices obtained from patients with MASLD at fibrosis stages F1 and F2, we found that Resmetirom reduced the PSR-positive area by 20% (Fig. 7D, E). Furthermore, in liver slices from MASLD patients with existing fibrosis and/or inflammation, Resmetirom increased the level of active form of MMP2 (Matrix Metalloproteinase-2 / Gelatinase A) protein while decreasing the level of TIMP1 (Fig. 7F, G). Together with the downregulation of profibrotic mediators, including components of the TGF-β signaling pathway, *CCN2, PDGFRB, ACTA2* and *COL1A1*, these findings suggest that treatment shifts ECM remodeling toward a matrix-degradative state, potentially promoting the breakdown of existing fibrotic collagen.

Discussion

From these studies, we draw four conclusions as depicted in graphical abstract regarding the underlying mechanisms to explain the beneficial effects of Resmetirom on the major components of disease of MASLD/MASH in patients at distinct stages of disease (Table 1). First, as shown in Fig. 1 and Fig. 2, Resmetirom reduces lipid accumulation in mild to severe hepatic steatosis and triglyceride synthesis by upregulating FAO related CPT1A and FGF21 genes, indicating that it activates hepatic THRβ to suppress lipogenesis and promote FAO [30, 31].

Second, Resmetirom enhances mitochondrial function by increasing mitochondria biogenesis, improving ATP synthesis and promoting oxidative phosphorylation (Fig. 1; Fig. 2). Resmetirom activates THRβ to upregulate *Prkab1* and *Ppargc1b* genes and mitochondrial ETC components in mouse PCLSs. In parallel, Resmetirom increased ATP production in patient PCLSs. RNA-seq

results suggest that Resmetirom promotes mitochondrial biosynthesis and oxidative metabolism by activating the AMPK-ERRα-PGC-1α signaling pathway by its actions on THRβ [32]. Resmetirom enhances the activity of the energy-sensing enzyme AMPK by upregulating *PRKAA1/PRKAB1*, consistent with enhanced AMPK pathways capacity. This activation shifts the liver from an anabolic (fat-storing) state to a catabolic (fat-burning) state [33, 34]. PGC-1α (*PPARGC1A*) and PGC-1β (*PPARGCIB*) as a coactivator works in tandem with ERRα to induce the expression of nuclear and mitochondrial genes that increase the number and efficiency of mitochondria [35]. Together, these changes support enhanced mitochondrial biogenesis, mitochondrial respiratory capacity and energy efficiency supporting improved hepatic metabolic function in MASLD/MASH.

Third, Resmetirom can not only reduce fibrosis progression but also promote fibrosis degradation. Stimulation of patient-derived PCLSs with TGFβ1/PDGF can induce reproducible fibrosis within a relatively short period (3 days), providing a rapid model for testing potential anti-fibrotic drugs in physiologically functional patient liver tissue. Resmetirom inhibits HSC activation and reverts activated HSCs to a quiescent state, thereby reducing fibrogenesis in human MASLD livers at fibrotic stages of up to F4 (Figs.3-6). Notably, its effects were observed not only in livers with normal histology (F0) or mild to moderate fibrosis (F1–F2), but also in livers with advanced fibrosis (F3–F4), including those from patients with varying degrees of MASH severity (Fig. 4). Importantly, PSR staining revealed that Resmetirom treatment alone reduced collagen deposition in liver slices from HFD-fed mice and patients with MASLD/MASH (Fig. S2; Fig. 7), suggesting a potential direct effect on hepatic fibrotic remodeling. These findings are consistent with recent AI-based digital pathology analyses of the phase III MAESTRO-NASH trial (NCT03900429), which demonstrated significant improvements in quantitative fibrosis (qFibrosis) scores with

Resmetirom versus placebo at week 52, particularly in the portal region and chicken-wire fibrosis patterns [36]. Together, these preclinical, ex vivo, and clinical findings support the potential of Resmetirom to promote hepatic fibrosis remodeling and regression.

As supporting evidence, our work has shown that treatment with Resmetirom in PCLSs derived from both mice and patients leads to the broad downregulation of a range of profibrotic genes (Fig. 3; Fig. 7). This indicates that Resmetirom exerts an antifibrotic effect by targeting key pathways that drive HSC activation, proliferation, and matrix production. The inhibition of TGFB1, TGFB1I1, and CCN2 suggests that the drug blocks the canonical TGF-β signaling pathway and disrupts the profibrotic positive-feedback loop that sustains the myofibroblast phenotype [37]. Concurrent downregulation of PDGFRB expression implies an inhibition of PDGF-mediated HSC proliferation and survival, thereby limiting the expansion of the profibrotic cell population [38]. Specifically, protein expression of α-SMA and COL1A1 was reduced following treatment (Fig. 5; Fig. 6), indicating that Resmetirom can directly suppresses myofibroblast activation and reduces ECM deposition or tissue fibrosis [39, 40].

The balance between MMPs and TIMPs is a key determinant of ECM homeostasis in the liver. MMP2 and MMP9 degrade ECM components, including denatured collagens, type IV collagen, fibronectin, and laminin, facilitating tissue remodeling and cell migration. TIMP1 acts as a natural inhibitor that binds directly to active MMPs to block their activity [41, 42]. Previous studies have shown that MMP2 deficiency exacerbates liver fibrosis in mice and is associated with increased TIMP1 expression and type I collagen synthesis [43, 44]. Furthermore, TIMP1 silencing using siRNA attenuates fibrotic responses and downregulates key fibrosis-related genes, including *ACTA2*, *CCN2*, and TGFBR2 [45]. Interestingly, Resmetirom modulated MMP2 and TIMP1 expression only in fibrotic liver slices (Fig. 7), with no detectable effects in normal human liver

slices or isolated human primary HSCs (data not shown). These findings suggest that Resmetirom-mediated regulation of the MMP2/TIMP1 axis may depend on the pathological liver microenvironment and interactions among different hepatic cell types rather than direct effects on HSCs alone. This observation further highlights the value of patient-derived PCLSs in capturing disease-context-dependent regulation of ECM remodeling.

Fourth, Resmetirom robustly attenuated hepatic inflammation (Fig. 3; Fig. 7), as evidenced by coordinated downregulation of key pro-inflammatory cytokines and chemokine signaling axes. Reduced *IL1B* and *IL6* expression suggests inhibition of upstream inflammatory signaling pathways, such as NF-κB and JAK/STAT, which drive amplification of inflammatory responses [46, 47]. Suppression of the *CCL2/CCL5/CCR5* pathway suggests reduced infiltration and retention of inflammatory macrophages [48], while decreased expression of interferon-inducible chemokines (CXCL9/*CXCL10*/*CXCL11*) indicates dampened immune cell activation and inflammatory crosstalk [49, 50]. These changes are consistent with reduced macrophage–HSC crosstalk and consequent attenuation of fibrosis progression [51, 52]. Collectively, these findings indicate that THRβ activation by Resmetirom exerts broad anti-inflammatory effects that likely interrupt the feed-forward loop linking hepatic inflammation to HSC activation and fibrogenesis, thereby contributing to disease modification in MASH. While we observed reductions in cytokine and chemokine levels following treatment, these measurements reflect changes in inflammatory signaling and do not directly indicate alterations in immune cell composition or spatial distribution within the tissue. Additional approaches, such as immunohistochemistry or spatial transcriptomics, would be required to determine whether immune cell populations or localization are affected in future study.

The *ex vivo* results were generated in patient-derived PCLSs using single, well-defined perturbations that model discrete clinical insults. By design, such reductionist assays do not fully recapitulate human MASLD, which develops over years under concurrent metabolic stressors, such as hyperinsulinemia, lipotoxicity, oxidative and inflammatory signals. This may in part explain why our *ex vivo* results had such high success rates compared to the lower success rates observed in clinical trials [7]. Accordingly, the magnitude of Resmetirom's effects *in vitro* may not translate directly *in vivo*. Even so, PCLSs provide a genuine pre-clinical translational platform to pinpoint drug-responsive pathways, identify which disease components, such as steatosis, mitochondrial dysfunction, and HSC activation/fibrogenesis, are modulated, and mitigate development risk before proceeding to costly clinical trials. Future work should incorporate combinatorial and/or chronic exposure (which would require longer culture strategies for PCLS) to better mimic the human milieu and to refine dosing and responder selection.

Abbreviations

Col1A1 Collagen type I alpha 1
DEGs Differentially expressed genes
DNL de novo lipogenesis
ECM Extracellular matrix
ETC Electron transport chain
FAO Fatty acid oxidation
GFP Green fluorescent protein
H&E Hematoxylin and eosin
HSC Hepatic stellate cell
MASH Metabolic dysfunction-associated steatohepatitis
MASLD Metabolic dysfunction-associated steatotic liver disease
MSD Meso Scale Discovery
OXPHOS Oxidative phosphorylation

PCLSs	Precision-cut liver slices
PFC	Perfluorocarbon
PSR	Picrosirius red
qPCR	Quantitative PCR
RNA-seq	RNA Sequencing
THRβ	Thyroid hormone receptor β
WB	Western blot

Supplementary information

Supplementary material 1: Fig. S1. Resmetirom blocks hepatic stellate cell activation in mouse hepatic stellate cells and LX2 cell line. (A) The images (40x objective) show that αSMA expression was detected in single hepatic stellate cells isolated from Col1A1-GFP mouse liver. scale bars = 20 μm. (B) A human LX2 stellate cell line was transfected with lenti-Col1A1-GFP to generate a stable cell line for testing fibrosis and anti-fibrotic treatments. scale bars = 20 μm. (C) Statistical results show the mean fluorescence intensity in LX2 cells. All the values are mean ± SEM; *$p<0.05$ by unpaired student's t-test. Fig. S2. Resmetirom can directly alleviate established fibrosis in livers of HFD-fed mice. (A) H&E and PSR stained images of liver slices from mice fed a high-fat diet (HFD) that exhibited fibrosis. PCLS prepared from these mice with established fibrosis were treated with or without Resmetirom (50 μM) for 4 days. Scale bar=200 μm. (B) PSR-positive area quantification. Resmetirom significantly reduced the PSR-positive rate (a 30% reduction). The value is mean ± SEM; *$p<0.05$ by unpaired student's t-test.

Supplementary material 2: RNA-seg data from mice.
Control vs Resmetirom treatment DEGs from mouse liver slices.

Supplementary material 3: RNA-seq data from MASLD patients.
Control vsResmetirom treatment_Human gene expression

Supplementary material 4: Resmetirom graphical figure.

Supplementary material 5: The full uncropped Gel and Blot images.

Acknowledgements

Some of the equipment used in this study was supported by the 3D (Diet, Digestive Tract and Disease) Centre funded by the Canadian Foundation for Innovation and Ontario Research Fund, project number 19442, and the Imaging Facility and SPARC Drug Discovery Core Facility at The Hospital for Sick Children (Toronto, Canada) for assistance with imaging and virus packaging. We

thank the Integrative Liver Cell Core (ILCC) of University of Southern California (R24AA012885) led by Dr. Hidekazu Tsukamoto, which stores the Col1A1-GFP mice that were originally obtained from Dr. David Brenner of UC San Diego. J.D-B was supported by NIH grants 1R01DK138210-01, 1R01DK130846-01 and U01DK120393; and Breakthrough T1D 3-SRA-2024-1518-S-B. M.M.F.Q was supported by National Institutes of Health grant K99DK140067. K.X. was supported by the National Science Foundation of China (82570710) for establishing of LX2-Col1A1-GFP cells. D.A.Y. was supported by the Canada Research Chairs Program. The graphical abstract was created in BioRender (https://BioRender.com).

Declarations

Fundings

This work was supported by the Canadian Institute of Health Research (CIHR PJT-186151), Diabetes Canada (OG-3-22-5687-HG) and the Canada Research Chairs Programme to H.Y.G.

Conflict of interests

All authors declare no competing interests.

Data availability

Raw count data are available in supplemental data.

Author contributions

L.X. designed the study, performed experiments, conducted data analysis and wrote the manuscript. X.N., S.H. and K.K. collected patient samples. X.N., H.J. L.C., and L.Z. performed some experiments and data analysis. T.L., F.K., T.T., T.Q., and X.H. assisted with experiments. Y.G., K.S., and M.M.F.Q. assisted with RNA-seq data analysis. D.D., D.W., and S.W. evaluated patient histology. J.D-B. and M.M.F.Q. contributed to the PFC dish culture concept. K.X. provided LX2-Col1A1-GFP cells. T.J., A.O., and O.R. provided patient liver samples. D.A.Y., H-K.S., and

J.A. assisted with study supervision. K.S. assisted with manuscript revision. H.G. conceived and designed the study, supervised the work, and co-wrote the manuscript.

Table 1. Patient information for the individuals included in this study is summarized.

ID	Sex	Age	BMI	T2D	Macrovesicular Steatosis	NAS	Lobular Inflammation	Ballooning	Portal inflammation	Fibrosis
1	F	40	60.5	Yes	10%	3/8	1/3	1/2	1/3	3/4
2	F	37	36.38	No	40%	3/8	1/3	0/2	0/3	0/4
3	F	38	62.4	No	5%	1/8	0/3	0/2	0/3	1/4
4	F	28	53.8	No	<5%	0/8	0/3	0/2	0/3	0/4
5	F	49	38.66	No	20%	2/8	1/3	0/2	1/3	0/4
6	F	51	41.74	No	40%	4/8	1/3	1/2	1/3	1/4
7	F	46	58.31	No	5%	1/8	0/3	0/2	0/3	0/4
8	F	49	44.35	Yes	0%	0/8	0/3	0/2	0/3	0/4
9	F	49	42.07	No	10%	1/8	0/3	0/2	1/3	0/4
10	F	42	48.07	Yes	20%	2/8	1/3	0/2	1/3	1/4
11	F	43	55.52	No	< 5%	0/8	0/3	0/2	0/3	1/4
12	F	50	54.38	No	5%	1/8	0/3	0/2	0/3	2/4
13	F	56	37.29	Yes	15%	2/8	1/3	0/2	1/3	2/4
14	F	60	42.11	No	30%	4/8	2/3	1/2	0/3	2/4
15	F	37	59.12	No	25%	4/8	2/3	1/2	1/3	2/4
16	F	64	48.03	No	10%	3/8	1/3	1/2	1/3	2/4
17	F	42	46.8	No	0%	0/8	0/3	0/2	1/3	0/4
18	F	22	55.72	No	10%	2/8	1/3	0/2	1/3	1/4
19	M	51	46.81	No	<5%	0/8	0/3	0/2	0/3	0/4
20	M	41	46.71	No	5%	2/8	1/3	0/2	1/3	1/4
21	F	53	40.04	Yes	20%	3/8	1/3	1/2	0/3	1/4
22	F	20	56.6	No	10%	3/8	1/3	1/2	1/3	1/4
23	F	48	45.54	No	50%	5/8	2/3	1/2	1/3	1/4
24	M	55	38.04	No	35%	6/8	2/3	2/2	1/3	4/4
25	F	51	39.8	No	50%	4/8	1/3	1/2	1/4	0/4
26	M	46	36.69	No	20%	2/8	1/3	0/2	0/3	1/4
27	M	64	46.64	Yes	35%	4/8	1/3	1/2	1/3	3/4
28	F	42	49	Yes	5%	1/8	0/3	0/2	0/3	1/4
29	M	34	39.04	Yes	60%	5/8	2/3	1/2	1/3	2/4
30	M	53	42.1	No	5%	3/8	1/3	1/2	0/3	1/4
31	F	57	38.07	No	5%	2/8	1/3	0/2	1/3	0/4
32	F	50	37.23	No	40%	4/8	1/3	1/2	1/3	1/4
33	F	33	61.86	No	20%	3/8	1/3	1/2	1/3	0/4
34	F	44	71.72	No	<5%	0/8	0/3	0/2	1/3	0/4
35	F	40	36.17	No	0%	0/8	0/3	0/2	0/3	0/4
36	F	37	48.5	No	60%	5/8	2/3	1/2	0/3	2/4
37	F	44	38.6	No	25%	3/8	1/3	1/2	1/3	2/4
38	M	37	42	No	10%	3/8	1/3	1/2	1/3	2/4
39	F	32	50	No	30%	1/2	1/3	1/2	1/3	2/4
40	F	40	51	No	0%	0/2	0/3	0/2	1/3	0/4
41	M	40	44.9	No	20%	4/8	2/3	1/2	1/3	1/4
42	M	39	39.2	No	5%	2/8	1/3	0/2	1/3	1/4
43	M	35	53.96	No	40%	6/8	3/3	1/2	1/3	2/4
44	F	44	58.58	No	30%	4/8	2/3	1/2	1/3	2/4
45	F	56	44.37	No	20%	4/8	2/3	1/2	1/3	2/4
46	F	39	51.44	No	5%	2/8	1/3	0/2	1/3	0/4
47	F	42	42.08	No	0%	0/8	0/3	0/2	1/3	0/4

Based on the staining images, the liver pathologists evaluated the samples using the Brunt system and summarized the data for macrovesicular steatosis (%), MASLD activity score (NAS), steatosis grade, lobular inflammation (0 – 3), ballooning (0 – 2), portal inflammation (0 – 3), and fibrosis stage (0 – 4). MASLD was diagnosed if the liver had >5% steatosis, and MASH was confirmed when ballooning of hepatocytes was present. Fibrosis stage was designated according to the Brunt scoring system (F0 to F4), where stage 0 = no fibrosis, stage 1 = mild fibrosis, stage 2 = moderate fibrosis, stage 3 = severe fibrosis, and stage 4 = cirrhosis. Interpretation of liver slides are limited to the above parameters only and are not intended for diagnosis or treatment of clinical disease. BMI, body mass index; T2D, type 2 diabetes; NAS: NAFLD Activity Score.

Figure legends

Fig. 1. Resmetirom reduces lipid accumulation and enhances mitochondrial function and biogenesis in hepatocytes of healthy mouse liver slices. (A) PCLSs were cultured in PFC based system. (B) Albumin (ng/mL) production levels in mouse PCLSs cultured in PFC or regular 35-mm dishes (n = 2 technical replicates from 3 mice). (C) Images of mouse liver slices show lipid droplets that are fluorescent after staining with BODIPY (n = 3 mice). Scale bars = 10 μm. (D) Statistical analysis of lipid accumulation and lipid droplet size. (E) Triglyceride assay in mouse liver slices normalized to 1 mg tissue. (F) Images show mouse PCLSs left untreated (control) or treated with 5 mM acetaminophen to induce mitochondria damage. 50 μM Resmetirom was added 12 hours after acetaminophen treatment of liver slices. Scale bars = 10 μm. (G) Statistical analysis shows the green and red fluorescence intensity. The mean fluorescence intensity ratio of GFP/mCherry was normalized to the control condition (n = 4 mice). (H) Resmetirom upregulates gene expression related to fatty acid oxidation and mitochondrial function in mouse PCLS (n = 4 mice). (I) Module scores were computed from global OXPHOS gene set. p value from a two-sided Wilcoxon test. (J) PCA ratio of control and Resmetirom-treated groups. (K) A volcano plot was used to visualize differential gene expression between the control and Resmetirom treatment groups. (L) Dot plot of enriched GO biological processes and KEGG pathways among DEGs. All the values are mean ± SEM. *p<0.05; **p<0.01; ***p<0.001 by student's t test.

Fig. 2. Resmetirom reversed lipid accumulation and improved mitochondria function in liver slices from obese patients undergoing bariatric surgery. (A) H&E staining shows liver morphology change from different culture day (patient ID: 43). (B) Albumin production assay from cultured patient liver slices (n = 4 patients; IDs: 40, 45-47). (C) H&E staining shows liver morphology from donor 1, 2, and 3 (left, 20x objective, scale bar = 100 μm). Lipid droplets were visualized by green BODIPY staining. 60x objective, Scale bars = 10 μm. (D) Statistical analysis shows both lipid accumulation and lipid droplet size in liver samples from patients with very mild, mild, and severe steatosis. The donor information is as follows: Donor 1 (ID: 4), Donor 2 (ID: 5), and Donor 3 (ID: 6). (E) Cellular ATP level from control and Resmetirom treated MASLD/MASH patient PCLSs (n = 5 patients corresponding to the colored dots, 50 μM resmetirom for 24 h). (F) Resmetirom improves mitochondrial function by upregulating protein expression in ETC complex V and III from patient PCLSs (n = 4 patients corresponding to the colored dots with IDs: 30, 31, 33, 34). All the values are mean ± SEM. *p<0.05; **p<0.01; ***p<0.001 by student's t test.

Fig. 3. Modeling fibrosis and testing antifibrotic therapy with Resmetirom in normal mouse PCLSs. (A) Representative 20x magnification images of H&E and PSR-stained PCLSs from three different mouse liver slices. Scale bars = 100 μm. (B) Image analysis of PSR-stained slices. (C) Hydroxyproline contents in corresponding conditions. (D) qPCR results show relative mRNA expression levels of fibrosis markers (n = 4 mice). (E) Heatmaps show the relative mRNA expression levels (Z-score) of inflammatory and fibrotic genes between the control group and the Resmetirom-treated group in mouse PCLSs (n = 4 mice). (F) Module scores were computed from global inflammatory and fibrotic gene sets. p value from a two-sided Wilcoxon test. (G) GSEA analysis was performed on the sorted gene expression dataset from mouse RNA-seq data. All the values are mean ± SEM. *p<0.05; **p<0.01; ***p<0.001 by student's t test.

Fig. 4. Resmetirom reduced new fibrosis development in PCLSs from bariatric surgery patients at different stages of fibrosis (F1 to F4). (A) Representative 20x magnification images of H&E and PSR–stained PCLSs derived from patient livers with fibrosis stages F0–F3/4. Scale bars = 100 μm. The donor information is as follows: Donor 1 (ID: 7), Donor 2 (ID: 11), Donor 3 (ID: 14), and Donor 4 (ID: 1). (B) PSR-positive area quantification (n = 3 - 7 patients; F0 IDs: 2, 7-9, 46, 47; F1 IDs: 3, 10, 11, 26, 28, 41, 42; F2 IDs: 12-14, 29, 36, 37, 39; F3/F4 IDs: 1, 24, 27). (C) Average summary of (B) showing PSR trajectories across fibrosis stages. (D) Human pro-collagen 1A1 levels in patient PCLSs (n = 5 patients with IDs: 36, 38, 39, 40, 46). (E) αSMA-positive area quantification (n = 7 patients with IDs: 36-39, 42-44). (F) Representative IHC αSMA staining images (ID: 36-39). Scale bars = 100 μm. Each colored dot represents a patient across the conditions tested. All the values are mean ± SEM. *p<0.05, **p<0.01, ***p<0.001 by student's t test.

Fig. 5. Resmetirom blocks HSC activation in a mouse model with a fluorescent stellate cell activation reporter. (A) The images (20x objective) show that Col1A1 is expressed as a green fluorescence marker in HSCs of Col1A1-GFP mice. (B) Mean fluorescence intensity in each condition (n = 4 mice). (C) High-magnification imaging (60x objective) demonstrated α-SMA expression in HSCs from mice liver slices (n = 3 mice). (D) Single cell images (40x objective) further showed α-SMA expression in individual HSCs isolated from Col1a1-GFP mice (n = 3 mice). A second example of this data is in Figure S1A. (E) Statistical results of Col1A1 and αSMA expression, cell size and circularity (n = 15 - 30 cells from 3 mice). All image scale bars = 20 μm. All the values are mean ± SEM. *p<0.05; **p<0.01; ***p<0.001 by student's t test.

Fig. 6. Resmetirom inhibits the activation of human primary hepatic stellate cells (hHSCs). (A) Representative images of αSMA immunostaining from lenti-Col1A1-GFP infected hHSCs. (B) Statistic of fluorescence intensity, cell size and circularity changes (n = 50 - 100 cells). (C) WB results of αSMA expression levels (n = 3 hHSC preparations). (D) Human pro-collagen 1A1 levels in hHSCs cultured for 48 hours under DMSO control conditions, treatment with TGF-β1, or treatment with TGF-β1 combined with Resmetirom at concentrations of 1, 5, 10, 20, 30, 50, or 100 μM, respectively (n = 4 hHSC preparations). All the values are mean ± SEM. *p<0.05; **p<0.01; ***p<0.001 by student's t test.

Fig. 7. Resmetirom can directly reduce inflammation and fibrotic remodeling from patient liver slices. (A and B) In patient donors' PCLS, Resmetirom downregulates fibrotic (A) and inflammatory (B) gene expression (n = 4 patients with IDs: 15-17, 28). (C) MSD multiplex assays were used to assess changes in cytokine and chemokine secretion in the culture media from patient-derived liver slices (n = 5 patients with IDs: 30-34). (D) H&E and PSR stained images of liver biopsy sections with fibrosis stages 1 (ID: 37) and 2 (ID: 45) treated (or not, control) with Resmetirom. Scale bar = 200 μm. (E) PSR-positive area quantification of PCLS from n = 4 patient donors at F1 (ID: 41) and F2 (ID: 37, 38, 45) treated as in (E). (F, G) Resmetirom affects ECM remodeling proteins – specifically increases MMP2 and reduces TIMP1 (n = 3 patient donors with IDs: 32 (F1), 43 (F2), 44 (F2)). All the values are mean ± SEM. *$p<0.05$; **$p<0.01$; ***$p<0.001$ by student's t test.

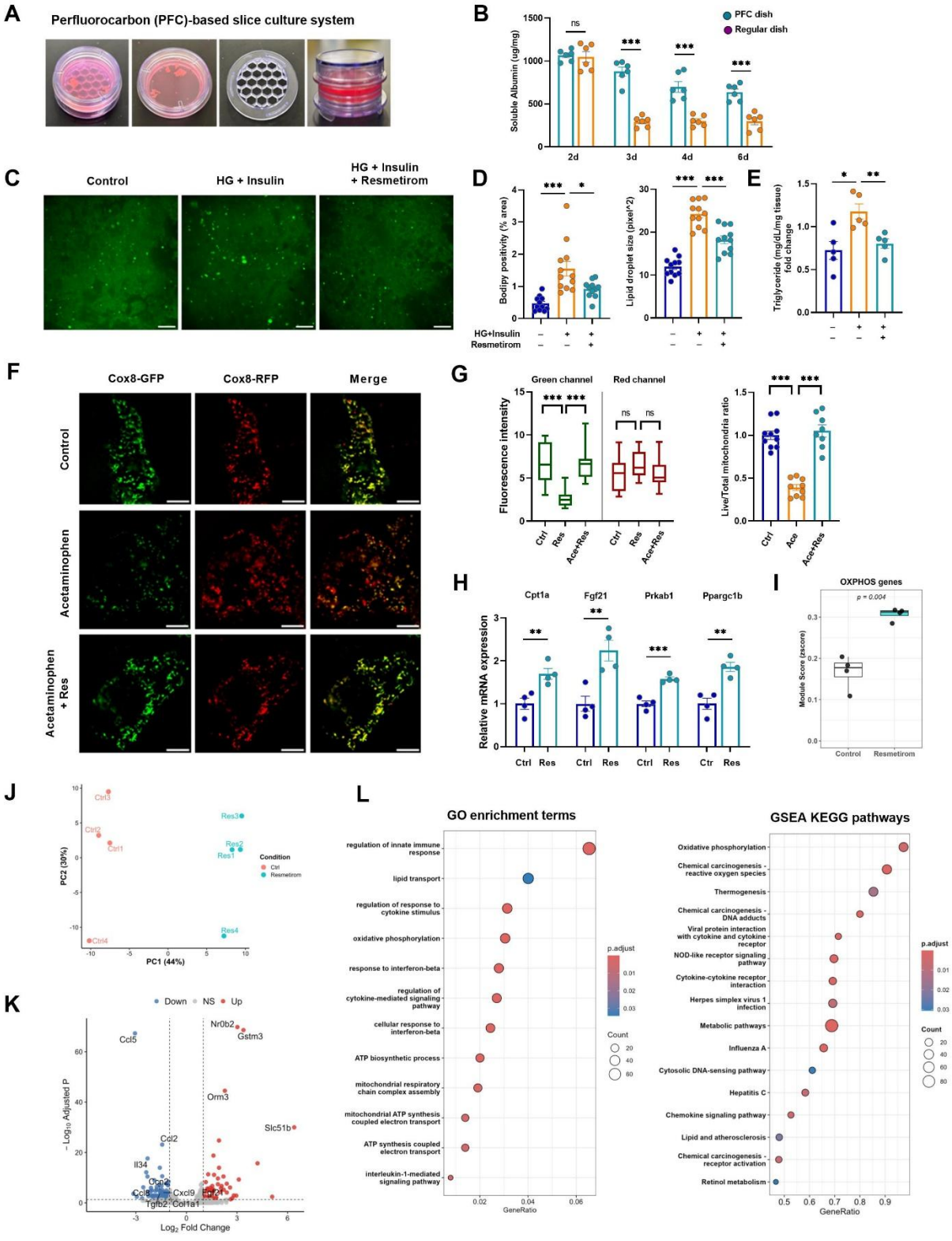

A
Perfluorocarbon (PFC)-based slice culture system
B
PFC dish
Regular dish
Soluble Albumin (ug/mg)
2d
3d
4d
6d
C
Control
HG + Insulin
HG + Insulin + Resmetirom
D
Bodipy positivity (% area)
Lipid droplet size (pixel^2)
HG+Insulin
Resmetirom
E
Triglyceride (mg/dL/mg tissue) fold change
F
Cox8-GFP
Cox8-RFP
Merge
Control
Acetaminophen
Acetaminophen + Res
G
Green channel
Red channel
Fluorescence intensity
Ctrl
Res
Ace+Res
Live/Total mitochondria ratio
Ace
H
Cpt1a
Fgf21
Prkab1
Ppargc1b
Relative mRNA expression
I
OXPHOS genes
p = 0.004
Module Score (zscore)
Control
Resmetirom
J
PC2 (30%)
PC1 (44%)
Condition
Ctrl
Resmetirom
K
Down
NS
Up
− Log10 Adjusted P
Log2 Fold Change
L
GO enrichment terms
regulation of innate immune response
lipid transport
regulation of response to cytokine stimulus
oxidative phosphorylation
response to interferon-beta
regulation of cytokine-mediated signaling pathway
cellular response to interferon-beta
ATP biosynthetic process
mitochondrial respiratory chain complex assembly
mitochondrial ATP synthesis coupled electron transport
ATP synthesis coupled electron transport
interleukin-1-mediated signaling pathway
GeneRatio
p.adjust
Count
GSEA KEGG pathways
Oxidative phosphorylation
Chemical carcinogenesis - reactive oxygen species
Thermogenesis
Chemical carcinogenesis - DNA adducts
Viral protein interaction with cytokine and cytokine receptor
NOD-like receptor signaling pathway
Cytokine-cytokine receptor interaction
Herpes simplex virus 1 infection
Metabolic pathways
Influenza A
Cytosolic DNA-sensing pathway
Hepatitis C
Chemokine signaling pathway
Lipid and atherosclerosis
Chemical carcinogenesis - receptor activation
Retinol metabolism

Figure 1

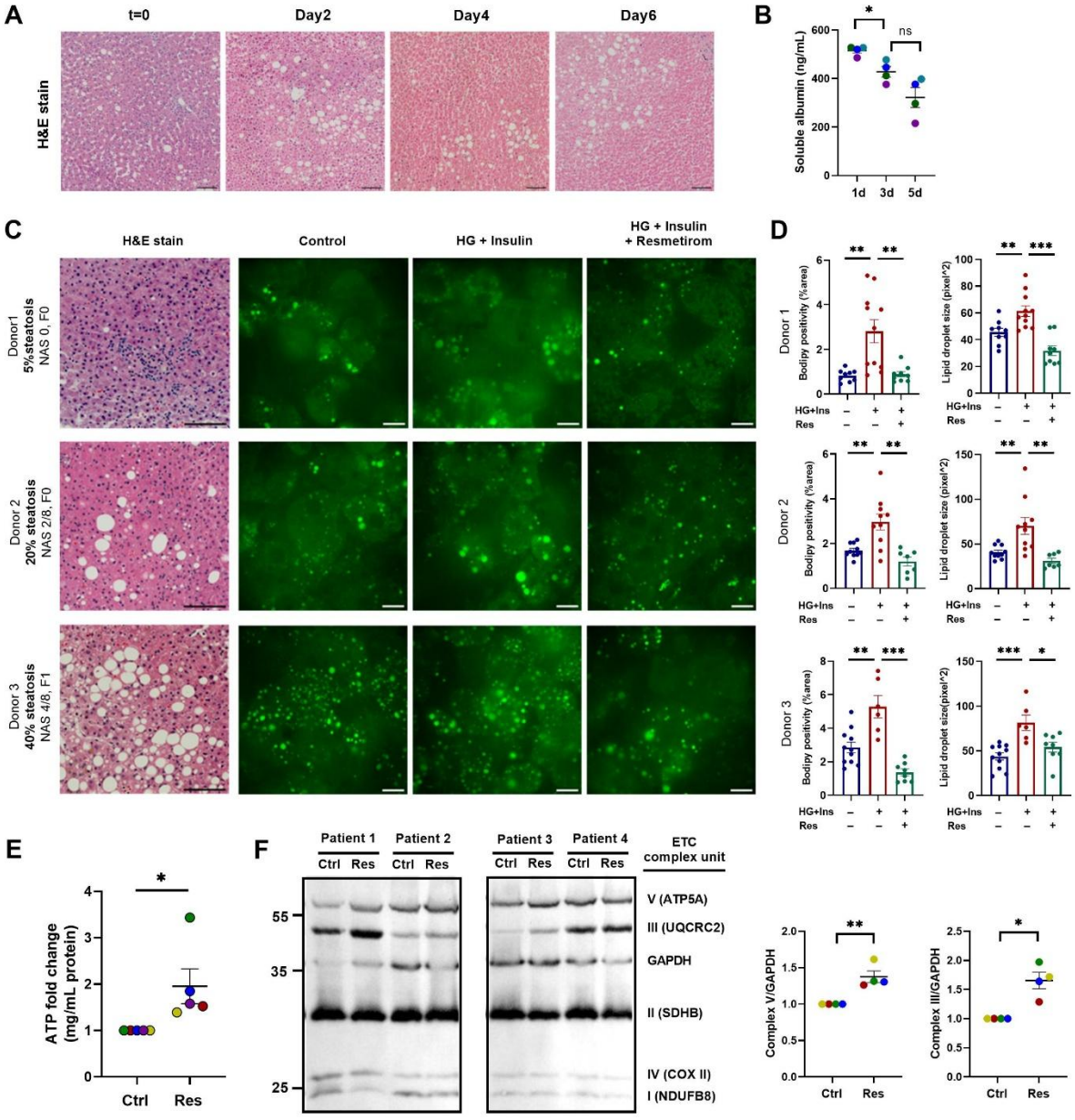

A
t=0
Day2
Day4
Day6
H&E stain
B
Soluble albumin (ng/mL)
1d
3d
5d
ns
C
H&E stain
Control
HG + Insulin
HG + Insulin + Resmetirom
Donor1 5%steatosis NAS 0, F0
Donor 2 20% steatosis NAS 2/8, F0
Donor 3 40% steatosis NAS 4/8, F1
D
Donor 1
Donor 2
Donor 3
Bodipy positivity (%area)
Lipid droplet size (pixel^2)
HG+Ins
Res
E
ATP fold change (mg/mL protein)
Ctrl
Res
F
Patient 1
Patient 2
Patient 3
Patient 4
Ctrl
Res
ETC complex unit
V (ATP5A)
III (UQCRC2)
GAPDH
II (SDHB)
IV (COX II)
I (NDUFB8)
55
35
25
Complex V/GAPDH
Complex III/GAPDH

Figure 2

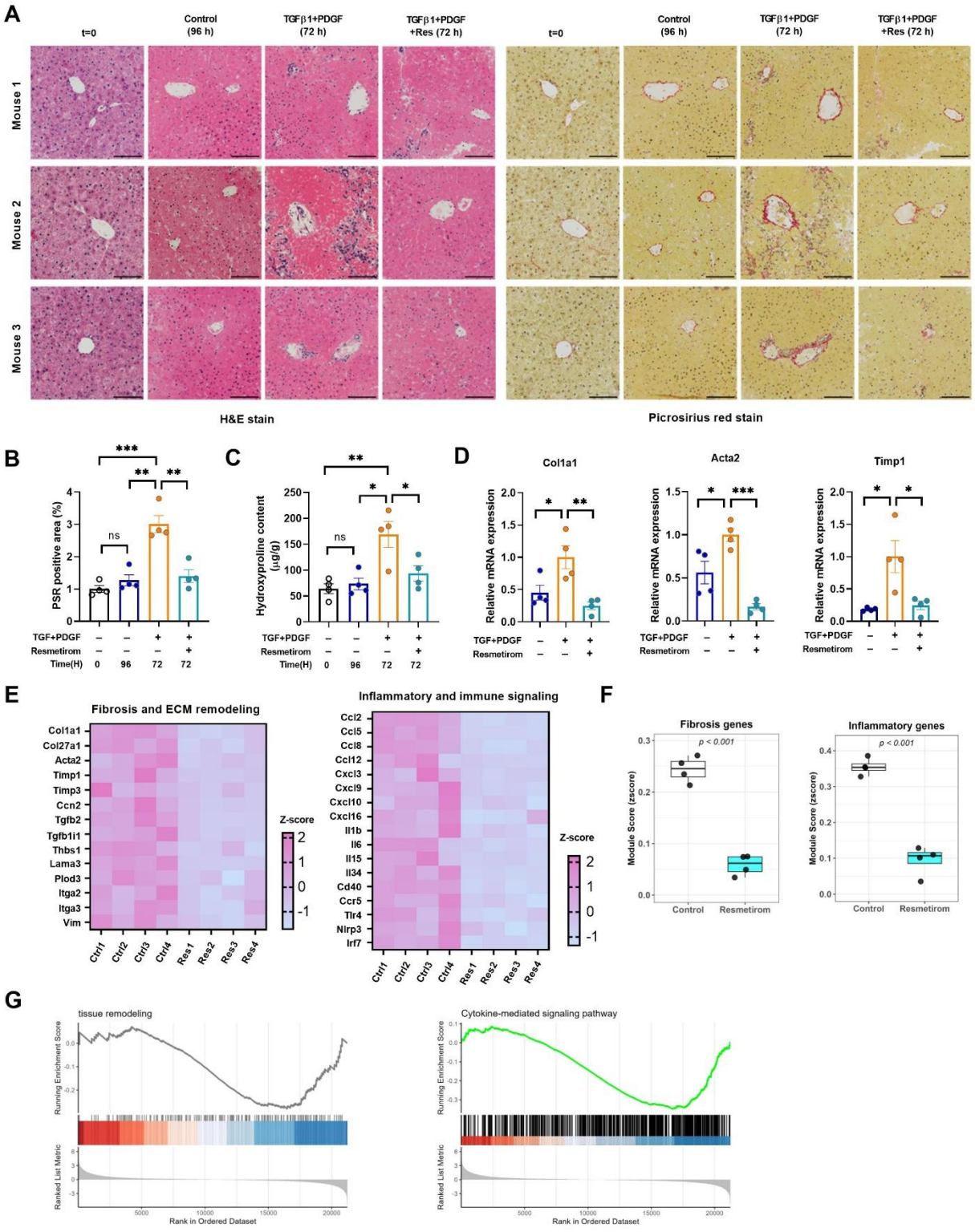

A
t=0
Control (96 h)
TGFβ1+PDGF (72 h)
TGFβ1+PDGF +Res (72 h)
Mouse 1
Mouse 2
Mouse 3
H&E stain
Picrosirius red stain
B
PSR positive area (%)
ns
TGF+PDGF
Resmetirom
Time(H) 0 96 72 72
C
Hydroxyproline content (μg/g)
D
Col1a1
Acta2
Timp1
Relative mRNA expression
E
Fibrosis and ECM remodeling
Col1a1
Col27a1
Acta2
Timp1
Timp3
Ccn2
Tgfb2
Tgfb1i1
Thbs1
Lama3
Plod3
Itga2
Itga3
Vim
Ctrl1 Ctrl2 Ctrl3 Ctrl4 Res1 Res2 Res3 Res4
Z-score
Inflammatory and immune signaling
Ccl2
Ccl5
Ccl8
Ccl12
Cxcl3
Cxcl9
Cxcl10
Cxcl16
Il1b
Il6
Il15
Il34
Cd40
Ccr5
Tlr4
Nlrp3
Irf7
F
Fibrosis genes
Inflammatory genes
p < 0.001
Module Score (zscore)
Control
Resmetirom
G
tissue remodeling
Cytokine-mediated signaling pathway
Running Enrichment Score
Ranked List Metric
Rank in Ordered Dataset

Figure 3

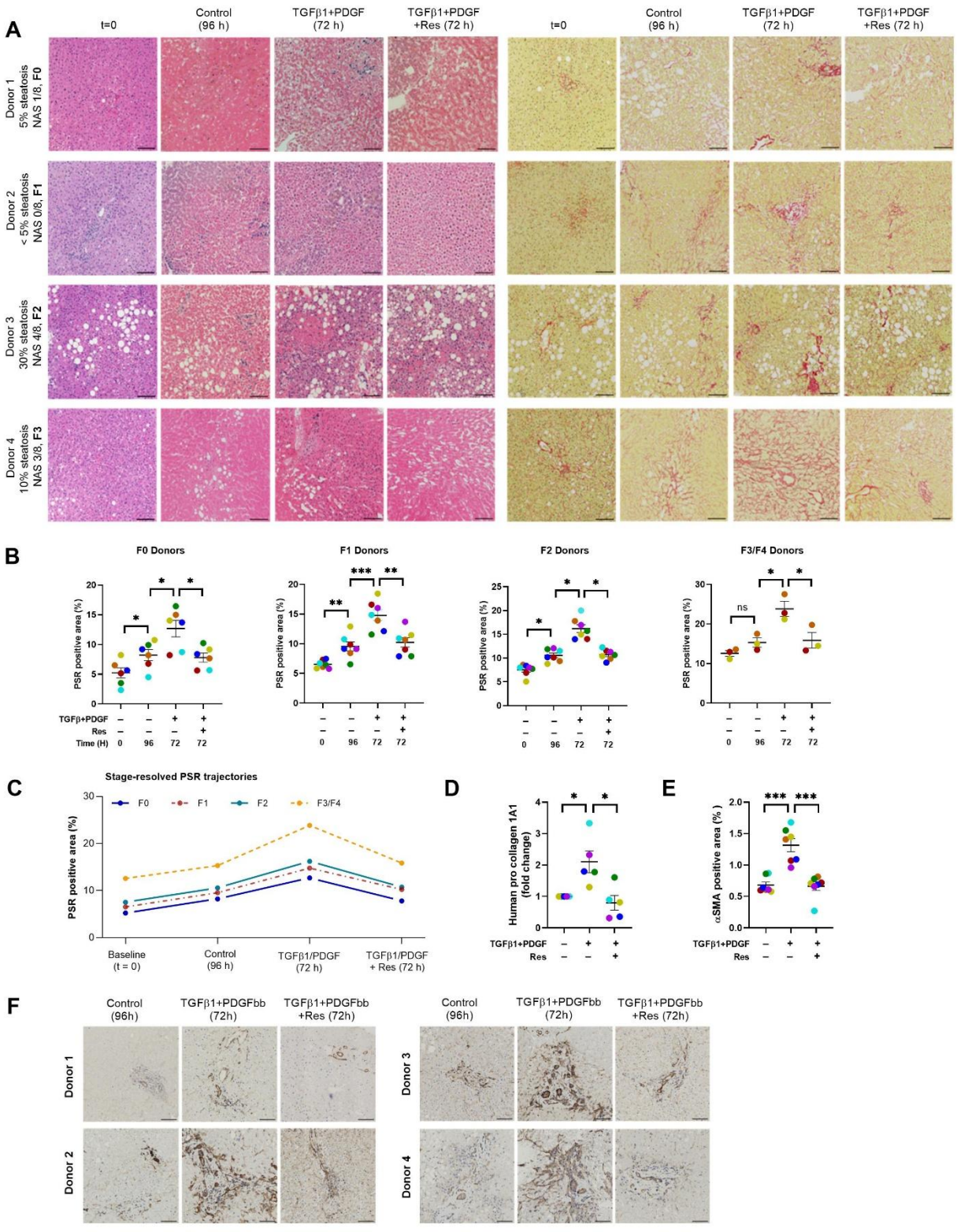

A
t=0
Control (96 h)
TGFβ1+PDGF (72 h)
TGFβ1+PDGF +Res (72 h)
Donor 1 5% steatosis NAS 1/8, F0
Donor 2 < 5% steatosis NAS 0/8, F1
Donor 3 30% steatosis NAS 4/8, F2
Donor 4 10% steatosis NAS 3/8, F3
B
F0 Donors
F1 Donors
F2 Donors
F3/F4 Donors
PSR positive area (%)
TGFβ+PDGF
Res
Time (H)
ns
C
Stage-resolved PSR trajectories
F0
F1
F2
F3/F4
Baseline (t = 0)
Control (96 h)
TGFβ1/PDGF (72 h)
TGFβ1/PDGF + Res (72 h)
D
Human pro collagen 1A1 (fold change)
E
αSMA positive area (%)
F
Control (96h)
TGFβ1+PDGFbb (72h)
TGFβ1+PDGFbb +Res (72h)
Donor 1
Donor 2
Donor 3
Donor 4

Figure 4

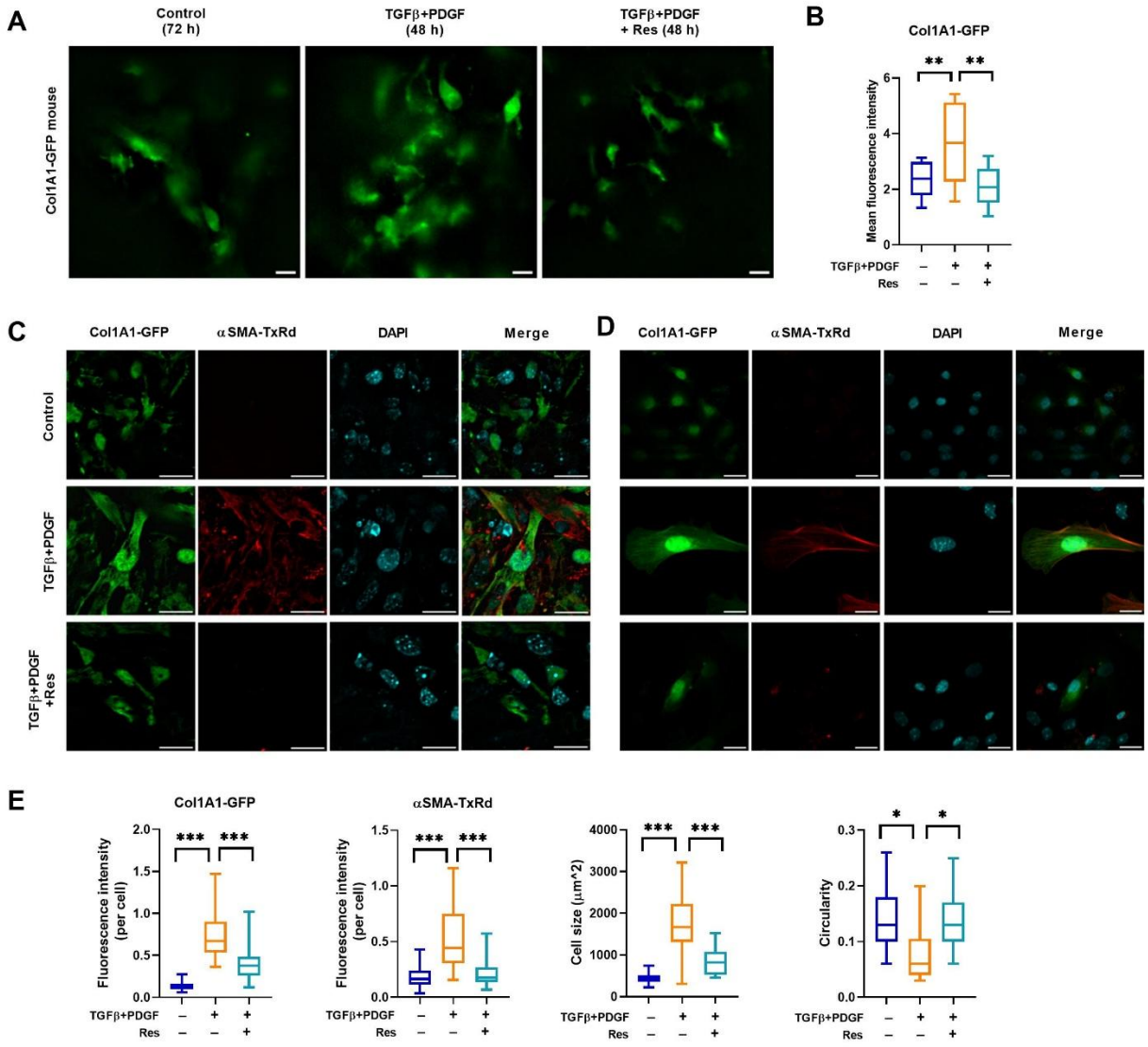

A
Control (72 h)
TGFβ+PDGF (48 h)
TGFβ+PDGF + Res (48 h)
Col1A1-GFP mouse
B
Col1A1-GFP
Mean fluorescence intensity
TGFβ+PDGF
Res
C
Col1A1-GFP
αSMA-TxRd
DAPI
Merge
Control
TGFβ+PDGF
TGFβ+PDGF +Res
D
E
Fluorescence intensity (per cell)
Cell size (μm^2)
Circularity

Figure 5

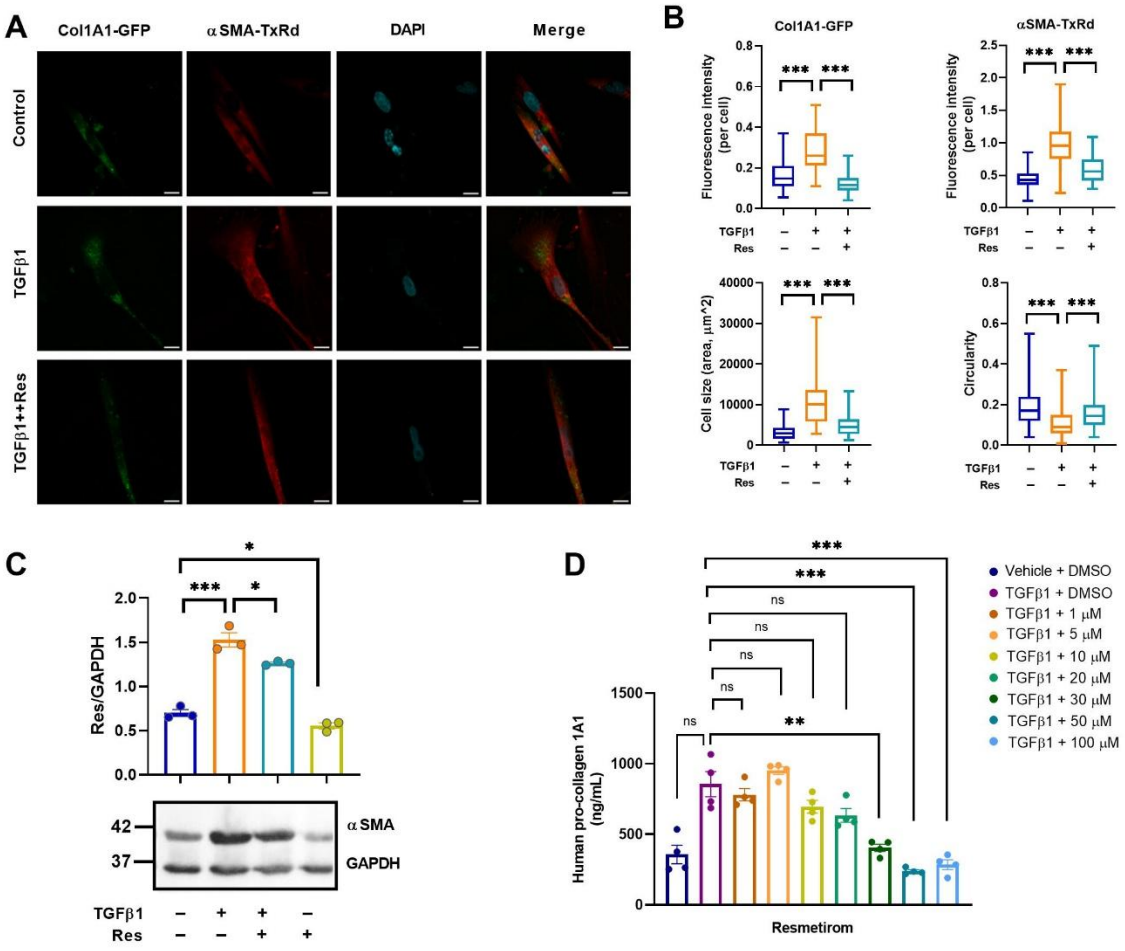

A
Col1A1-GFP
αSMA-TxRd
DAPI
Merge
Control
TGFβ1
TGFβ1++Res
B
Col1A1-GFP
αSMA-TxRd
Fluorescence intensity (per cell)
Cell size (area, μm^2)
Circularity
TGFβ1
Res
C
Res/GAPDH
αSMA
GAPDH
42
37
D
Human pro-collagen 1A1 (ng/mL)
Resmetirom
Vehicle + DMSO
TGFβ1 + DMSO
TGFβ1 + 1 μM
TGFβ1 + 5 μM
TGFβ1 + 10 μM
TGFβ1 + 20 μM
TGFβ1 + 30 μM
TGFβ1 + 50 μM
TGFβ1 + 100 μM

Figure 6

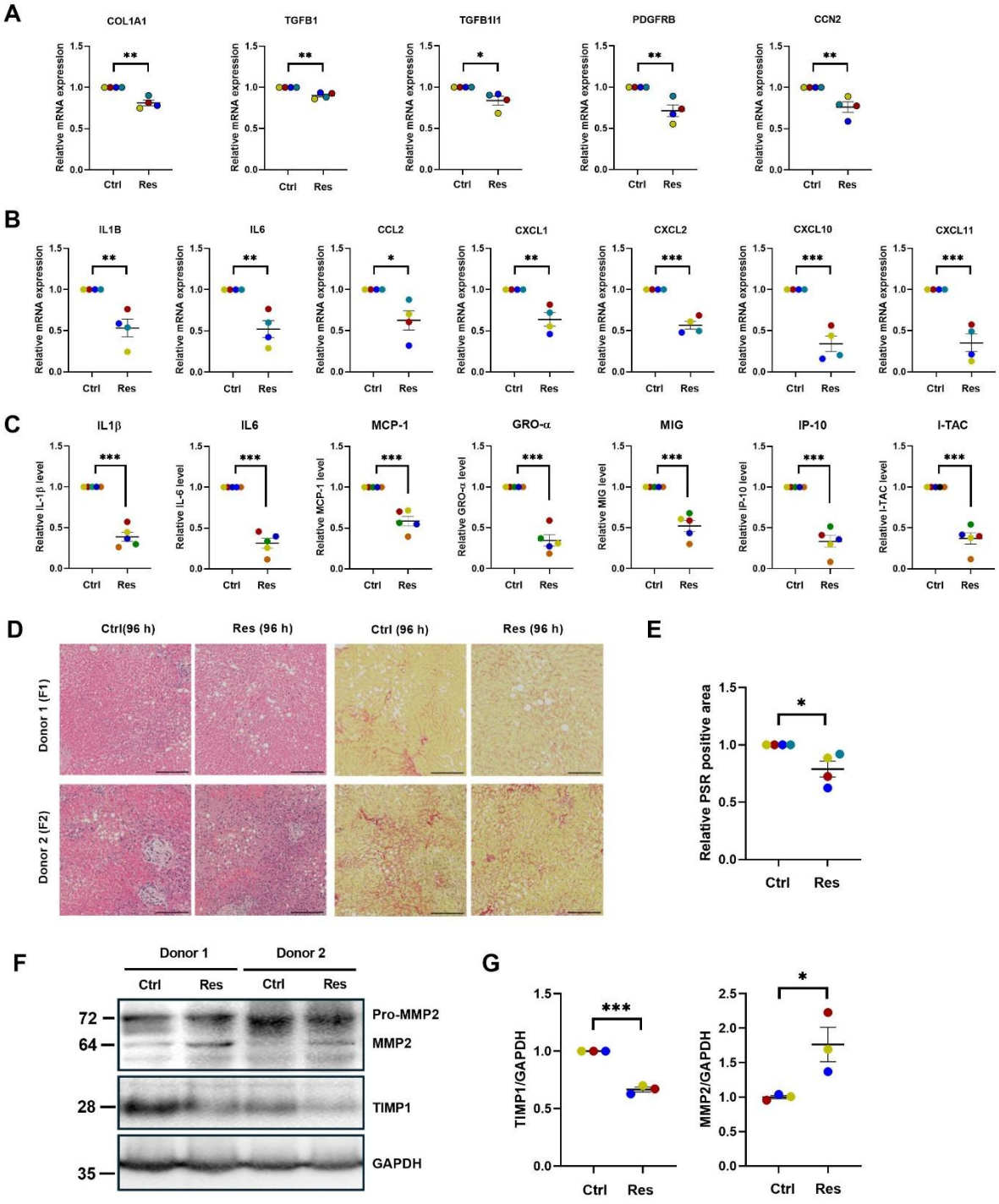

A
COL1A1
TGFB1
TGFB1I1
PDGFRB
CCN2
Relative mRNA expression
Ctrl
Res
B
IL1B
IL6
CCL2
CXCL1
CXCL2
CXCL10
CXCL11
C
IL1β
IL6
MCP-1
GRO-α
MIG
IP-10
I-TAC
Relative IL-1β level
Relative IL-6 level
Relative MCP-1 level
Relative GRO-α level
Relative MIG level
Relative IP-10 level
Relative I-TAC level
D
Ctrl(96 h)
Res (96 h)
Ctrl (96 h)
Res (96 h)
Donor 1 (F1)
Donor 2 (F2)
E
Relative PSR positive area
F
Donor 1
Donor 2
Pro-MMP2
MMP2
TIMP1
GAPDH
72
64
28
35
G
TIMP1/GAPDH
MMP2/GAPDH

Figure 7

References

1. Riazi K, Azhari H, Charette JH, et al. The prevalence and incidence of NAFLD worldwide: a systematic review and meta-analysis. The Lancet Gastroenterology & Hepatology 2022; 7, 851–861. 10.1016/s2468-1253(22)00165-0.

2. Sangro P, de la Torre Aláez M, Sangro B, et al. Metabolic dysfunction–associated fatty liver disease (MAFLD): an update of the recent advances in pharmacological treatment. Journal of Physiology and Biochemistry 2023;79, 869–879. 10.1007/s13105-023-00954-4.

3. Chen L, Tao X, Zeng M, et al. Clinical and histological features under different nomenclatures of fatty liver disease: NAFLD, MAFLD, MASLD and MetALD. Journal of Hepatology 2024; 80, e64–e66. 10.1016/j.jhep.2023.08.021.

4. Dougherty JA, Guirguis E, Thornby KA. A Systematic Review of Newer Antidiabetic Agents in the Treatment of Nonalcoholic Fatty Liver Disease. Annals of Pharmacotherapy 2020; 55, 65–79. 10.1177/1060028020935105.

5. Vincent RK, Williams DM, Evans M. A look to the future in non-alcoholic fatty liver disease: Are glucagon-like peptide-1 analogues or sodium-glucose co-transporter-2 inhibitors the answer? Diabetes, Obesity and Metabolism 2020; 22, 2227–2240. 10.1111/dom.14196.

6. Lassailly G, Caiazzo R, Ntandja-Wandji LC, et al. Bariatric Surgery Provides Long-term Resolution of Nonalcoholic Steatohepatitis and Regression of Fibrosis. Gastroenterology 2020; 159, 1290–1301.e1295. 10.1053/j.gastro.2020.06.006.

7. Harrison SA, Bedossa P, Guy C, et al. A Phase 3, Randomized, Controlled Trial of Resmetirom in NASH with Liver Fibrosis. New England Journal of Medicine 2024; 390, 497–509. 10.1056/NEJMoa2309000.

8. Sanyal AJ, Newsome PN, Kliers I, et al. Phase 3 Trial of Semaglutide in Metabolic Dysfunction–Associated Steatohepatitis. New England Journal of Medicine 2025;392, 2089–2099. 10.1056/NEJMoa2413258.

9. Wang X, Wang L, Geng L, et al. Resmetirom Ameliorates NASH-Model Mice by Suppressing STAT3 and NF-κB Signaling Pathways in an RGS5-Dependent Manner. International Journal of Molecular Sciences 2023;24.

10. Sookoian S, Pirola CJ. Resmetirom for treatment of MASH. Cell 2024;187, 2897–2897.e2891. 10.1016/j.cell.2024.05.009.

11. Hagström H, Nasr P, Ekstedt M, et al. Fibrosis stage but not NASH predicts mortality and time to development of severe liver disease in biopsy-proven NAFLD. Journal of Hepatology 2017; 67, 1265–1273. 10.1016/j.jhep.2017.07.027.

12. Starokozhko V, Vatakuti S, Schievink B, et al. Maintenance of drug metabolism and transport functions in human precision-cut liver slices during prolonged incubation for 5 days. Archives of Toxicology 2016;91, 2079–2092. 10.1007/s00204-016-1865-x.

13. Paish HL, Reed LH, Brown H, et al. A Bioreactor Technology for Modeling Fibrosis in Human and Rodent Precision-Cut Liver Slices. Hepatology 2019;70, 1377–1391. 10.1002/hep.30651.

14. Qadir, MMF, Álvarez-Cubela S, Weitz J, et al. Long-term culture of human pancreatic slices as a model to study real-time islet regeneration. Nature Communications 2020;11. 10.1038/s41467-020-17040-8.

15. Liang T, Dolai S, Xie L, et al. Ex vivo human pancreatic slice preparations offer a valuable model for studying pancreatic exocrine biology. Journal of Biological Chemistry 2017;292(14): 5957–5969.

16. Brunt EM, Janney CG, Di Bisceglie AM, et al. Nonalcoholic Steatohepatitis: A Proposal for Grading and Staging The Histological Lesions. American Journal of Gastroenterology 1999;94, 2467–2474. 10.1111/j.1572-0241.1999.01377.x.

17. Wang L, Jin XS, Dong HJ, et al. [Establishment of a reporter system for estimating activation of human hepatic stellate cells based on COL1A1 promoter and enhanced green fluorescent protein]. Beijing Da Xue Xue Bao Yi Xue Ban 2023;*55*, 876–885. 10.19723/j.issn.1671-167X.2023.05.016.

18. Syed-Abdul MM. Lipid Metabolism in Metabolic-Associated Steatotic Liver Disease (MASLD). Metabolites 2023;14. 10.3390/metabo1401001

19. Smith GI, Shankaran M, Yoshino M, et al. Insulin resistance drives hepatic de novo lipogenesis in nonalcoholic fatty liver disease. Journal of Clinical Investigation 2020;130, 1453–1460. 10.1172/jci134165.

20. Morio B, Panthu B, Bassot A, et al. Role of mitochondria in liver metabolic health and diseases. Cell Calcium 2021;*94*. 10.1016/j.ceca.2020.102336.

21. Jaeschke H, Duan L, Nguyen NT, et al. Mitochondrial damage and biogenesis in acetaminophen-induced liver injury. Liver Research 2019;3, 150–156. 10.1016/j.livres.2019.10.002.

22. Rojansky R, Cha MY, Chan DC. Elimination of paternal mitochondria in mouse embryos occurs through autophagic degradation dependent on PARKIN and MUL1. eLife 2016; 5. 10.7554/eLife.17896

23. Qadir MMF, Dana C, Mauvais-Jarvis P, et al. Supervised machine learning identifies impaired mitochondrial quality control in β cells with development of type 2 diabetes. bioRxiv 2025. 10.1101/2025.10.22.683335.

24. Kisseleva T, Ganguly S, Murad R, et al. Regulation of Hepatic Stellate Cell Phenotypes in Metabolic Dysfunction–Associated Steatohepatitis. Gastroenterology. 2025; 10.1053/j.gastro.2025.03.010.

25. Kolios G. Role of Kupffer cells in the pathogenesis of liver disease. World Journal of Gastroenterology 2006;12. 10.3748/wjg.v12.i46.7413.

26. Mihaylova Z, Tsikandelova R, Sanimirov P, et al. Role of PDGF-BB in proliferation, differentiation and maintaining stem cell properties of PDL cells in vitro. Archives of Oral Biology 2018;85, 1–9. 10.1016/j.archoralbio.2017.09.019.

27. Rippe RA, Lorenzen SI, Brenner DA, et al. Regulatory Elements in the 5′-Flanking Region and the First Intron Contribute to Transcriptional Control of the Mouse Alpha 1 Type I Collagen Gene. Molecular and Cellular Biology 1989 ;9, 2224–2227. 10.1128/mcb.9.5.2224-2227.

28. Novoa E, Cabaleiro A, López-Picallo B, et al. Resmetirom Ameliorates Fibrogenesis in Hepatic Stellate Cells via Thyroid Hormone Receptor Alpha-Fatty-Acid Amide Hydrolase 1 Signaling Pathway. MedComm. 2026;7. 10.1002/mco2.70901.

29. Matsumoto M, Hada N, Sakamaki Y, et al. An improved mouse model that rapidly develops fibrosis in non-alcoholic steatohepatitis. International Journal of Experimental Pathology 2013;*94*, 93–103. 10.1111/iep.12008

30. Sun W, Nie T, Li K, et al. Hepatic CPT1A Facilitates Liver–Adipose Cross Talk via Induction of FGF21 in Mice. Diabetes 2022;71, 31–42. 10.2337/db21-0363.

31. Cui X, Sun Q, Wang H. Targeting fibroblast growth factor (FGF)-21: a promising strategy for metabolic dysfunction-associated steatotic liver disease treatment. Frontiers in Pharmacology 2025;*6*. 10.3389/fphar.2025.1510322.

32. Herzig S, Shaw RJ. AMPK: guardian of metabolism and mitochondrial homeostasis. Nature Reviews Molecular Cell Biology 2017;*19*, 121–135. 10.1038/nrm.2017.95.

33. Desjardins EM, Smith BK, Day EA, et al. The phosphorylation of AMPKβ1 is critical for increasing autophagy and maintaining mitochondrial homeostasis in response to fatty acids. Proceedings of the National Academy of Sciences 2022). *119*. 10.1073/pnas.2119824119.

34. Smiles WJ, Ovens AJ, Oakhill JS, et al. The metabolic sensor AMPK: Twelve enzymes in one. Molecular Metabolism 2024;*90*. 10.1016/j.molmet.2024.102042.

35. Fisher KW, Das B, Kim HS, et al. AMPK Promotes Aberrant PGC1β Expression To Support Human Colon Tumor Cell Survival. Molecular and Cellular Biology 2023;*35*, 3866–3879. 10.1128/mcb.00528-15

36. Schattenberg JM, Bedossa P, Guy CD, et al. Quantitative regression of qFibrosis with resmetirom: Exploratory histologic endpoints from the MAESTRO-NASH phase III clinical trial. Journal of Hepatology 2026;85, 202–211. 10.1016/j.jhep.2026.03.021.

37. Györfi AH, Matei AE, Distler JHW. Targeting TGF-β signaling for the treatment of fibrosis. Matrix Biology 2018;68-69, 8–27. 10.1016/j.matbio.2017.12.016.

38. Kocabayoglu P, Lade A, Lee YA, et al. β-PDGF receptor expressed by hepatic stellate cells regulates fibrosis in murine liver injury, but not carcinogenesis. Journal of Hepatology 2015;63, 141–147. 10.1016/j.jhep.2015.01.036.

39. Devos H, Zoidakis J, Roubelakis MG, et al. Reviewing the Regulators of COL1A1. International Journal of Molecular Sciences 2023;24. 10.3390/ijms241210004.

40. Rockey DC, Du Q, Shi Z. Smooth Muscle α-Actin Deficiency Leads to Decreased Liver Fibrosis via Impaired Cytoskeletal Signaling in Hepatic Stellate Cells. The American Journal of Pathology 2019;189, 2209–2220. 10.1016/j.ajpath.2019.07.019.

41. Wolosowicz M, Prokopiuk S, Kaminski TW. The Complex Role of Matrix Metalloproteinase-2 (MMP-2) in Health and Disease. International Journal of Molecular Sciences 2024;25. 10.3390/ijms252413691.

42. Kazemi A, Fathy M, Jahanian A, et al. The role of MMPs and TIMPs in regenerative medicine: From pathological ECM remodeling to therapeutic applications. Biomedicine & Pharmacotherapy 2025;191. 10.1016/j.biopha.2025.118457.

43. Onozuka I, Kakinuma S, Kamiya A, et al. Cholestatic liver fibrosis and toxin-induced fibrosis are exacerbated in matrix metalloproteinase-2 deficient mice. Biochemical and Biophysical Research Communications 2011;406, 134–140. 10.1016/j.bbrc.2011.02.012.

44. Radbill BD, Gupta R, Ramirez MCM, et al. Loss of Matrix Metalloproteinase-2 Amplifies Murine Toxin-Induced Liver Fibrosis by Upregulating Collagen I Expression. Digestive Diseases and Sciences 2010;*56*, 406–416. 10.1007/s10620-010-1296-0.

45. Wang K, Lin B, Brems JJ, et al. Hepatic apoptosis can modulate liver fibrosis through TIMP1 pathway. Apoptosis 2013;18, 566–577. 10.1007/s10495-013-0827-5.

46. Schmidt-Arras D, Rose-John S. IL-6 pathway in the liver: From physiopathology to therapy. Journal of Hepatology 2016;64, 1403–1415. 10.1016/j.jhep.2016.02.004.

47. Mossman KL, Negash AA, Ramos HJ, et al. IL-1β Production through the NLRP3 Inflammasome by Hepatic Macrophages Links Hepatitis C Virus Infection with Liver Inflammation and Disease. PLoS Pathogens 2013;9. 10.1371/journal.ppat.1003330.

48. Marra F, Tacke F. Roles for Chemokines in Liver Disease. Gastroenterology 2014;147, 577–594.e571. 10.1053/j.gastro.2014.06.043.

49. Tokunaga R, Zhang W, Naseem M, et al. CXCL9, CXCL10, CXCL11/CXCR3 axis for immune activation – A target for novel cancer therapy. Cancer Treatment Reviews 2018;*63*, 40–47. 10.1016/j.ctrv.2017.11.007.

50. Ozga AJ, Chow MT, Lopes ME, et al. CXCL10 chemokine regulates heterogeneity of the CD8+ T cell response and viral set point during chronic infection. Immunity 2022;55, 82–97.e88. 10.1016/j.immuni.2021.11.002.

51. Wynn TA, Ramalingam TR. Mechanisms of fibrosis: therapeutic translation for fibrotic disease. Nature Medicine 2012;18, 1028–1040. 10.1038/nm.2807.

52. Taru V, Szabo G, Mehal W, et al. Inflammasomes in chronic liver disease: Hepatic injury, fibrosis progression and systemic inflammation. Journal of Hepatology 2024;81, 895–910. 10.1016/j.jhep.2024.06.016.

Supplementary Files

This is a list of supplementary files associated with this preprint. Click to download.

- ControlvsResmetiromtreatmentDEGsformmouseliverslices.csv
- ControlvsResmetiromtreatmentHumangeneexpression.xlsx
- ThefulluncroppedGelandBlotimagesResmetirom.pdf
- Resmetiromgraphicalfigure.pdf
- hgSupplementarymaterialResmetiromJTM.docx